

Robust Policy Switching for Antifragile Reinforcement Learning for UAV Deconfliction in Adversarial Environments

Deepak Kumar Panda¹ and Weisi Guo¹

Abstract—The increasing automation of navigation for unmanned aerial vehicles (UAVs) has exposed them to adversarial attacks that exploit vulnerabilities in reinforcement learning (RL) through sensor manipulation. Although existing robust RL methods aim to mitigate such threats, their effectiveness has limited generalization to out-of-distribution shifts from the optimal value distribution, as they are primarily designed to handle fixed perturbation. To address this limitation, this paper introduces an antifragile RL framework that enhances adaptability to broader distributional shifts by incorporating a switching mechanism based on discounted Thompson sampling (DTS). This mechanism dynamically selects among multiple robust policies to minimize adversarially induced state-action-value distribution shifts. The proposed approach first derives a diverse ensemble of action-robust policies by accounting for a range of perturbations in the policy space. These policies are then modeled as a multiarmed bandit (MAB) problem, where DTS optimally selects policies in response to nonstationary Bernoulli rewards, effectively adapting to evolving adversarial strategies. Theoretical framework has also been provided where by optimizing the DTS to minimize the overall regrets due to distributional shift, results in effective adaptation against unseen adversarial attacks thus inducing antifragility. Extensive numerical simulations validate the effectiveness of the proposed framework in complex navigation environments with multiple dynamic three-dimensional obstacles and with stronger projected gradient descent (PGD) and spoofing attacks. Compared to conventional robust, non-adaptive RL methods, the antifragile approach achieves superior performance, demonstrating shorter navigation path lengths and a higher rate of conflict-free navigation trajectories compared to existing robust RL techniques.

Index Terms—Adversarial Attacks, Reinforcement Learning, UAV, Navigation, Thompson Sampling.

I. INTRODUCTION

Unmanned aerial vehicles (UAVs) have become pivotal in tasks such as aerial surveillance [1, 2], target tracking [3], reconnaissance [4], and logistics [5]. As their deployment in civil airspace expands, ensuring safe and conflict-free navigation is critical [6], necessitating robust unmanned aircraft traffic management (UTM) systems [7]. According to ICAO [8], conflict detection and resolution (CDR) in UTM operates across three layers: *strategic conflict management* (pre-flight deconfliction) [9, 10], *separation provision* (in-flight tactical

decisions) [11, 12], and *collision avoidance* (post-conflict mitigation) [13]. While strategic deconfliction offers early conflict prevention, it lacks flexibility to handle sudden changes like airspace closures. Tactical deconfliction, by contrast, supports real-time adaptation through onboard sensors and surveillance technologies.

Reinforcement learning (RL) has emerged as a promising tool for tactical deconfliction [14, 15], enabling UAVs to adapt to real-time conditions by learning optimal control policies in high-dimensional state-action spaces. However, RL policies are heavily reliant on sensor data and communication channels, which are vulnerable to adversarial attacks such as spoofing, jamming, and evasion [16–19]. These threats not only degrade perception but can also exploit the RL agent’s policy directly [20, 21].

To address these challenges, this paper explores an *antifragile* RL framework for UAV tactical deconfliction under adversarial attacks. Rather than merely withstanding disruptions, the proposed method adapts and improves from them by leveraging an ensemble of robust policies and dynamically selecting among them using distributional feedback. Our approach integrates adversarially trained policies with Discounted Thompson Sampling (DTS) to adaptively switch to the most robust policy in response to unseen perturbations, enhancing both safety and resilience in UTM environments.

A. Related Works

1) Tactical UAV Deconfliction

Traditional deconfliction approaches combine trajectory optimization with cost functions that adapt to dynamic environments. Rule-based planners such as A* [22], Dijkstra’s algorithm [23], and artificial potential fields (APF) [24] offer limited adaptability in real time. More sophisticated frameworks using model predictive control (MPC) [25] and mixed-integer linear programming (MILP) [26] improve obstacle avoidance but remain computationally intensive and often limited to 2D environments.

Reinforcement learning (RL) offers a scalable alternative for 3D tactical deconfliction by optimizing policies over high-dimensional state spaces. However, existing RL-based methods often struggle with generalization under adversarial perturbations. To enhance efficiency and safety in 3D navigation, fluid dynamics-based trajectory planning, such as interfered fluid dynamics systems (IFDS) [27, 28], has been used to incorporate UAV kinematics and reduce path cost [29]. Recent work integrating IFDS with deep RL has

This work was supported by the Royal Academy of Engineering and the Office of the Chief Science Adviser for National Security under the UK Intelligence Community Postdoctoral Research Fellowship programme

¹The authors are with Faculty of Engineering and Applied Sciences, Cranfield University, MK43 0AL Cranfield, U.K. Deepak.Panda@cranfield.ac.uk, weisi.guo@cranfield.ac.uk

shown improved resilience and adaptability [30]. Building upon this, our approach enhances RL-based deconfliction by incorporating adaptive policy switching to counter adversarial threats.

2) Adversarial Threats and Robust RL Defenses

Adversarial attacks in RL are commonly categorized into perturbations of the state, action, model, and reward spaces [20, 31, 32]. State-space attacks use gradient-based loss functions [33] or saliency maps [34] to mislead perception. Action-space and model-space attacks manipulate policy behavior and model integrity [35, 36], while reward-space attacks distort agent learning [19, 37]. Defensive strategies include adversarial training [33, 38], defensive distillation [39, 40], and risk-aware modeling [41, 42]. These methods enhance robustness by preparing agents for known perturbation types. Other techniques include noisy reward shaping [43], falsified temporal logic constraints [44], and adversary-aware training [45].

However, most robust RL approaches assume stationary or bounded distribution shifts. When exposed to previously unseen or evolving threats, their performance often degrades due to lack of adaptability. Static defenses cannot dynamically respond to adversarial strategies that change over time. Our work addresses this limitation by inducing adaptability through policy switching, enabling the agent to operate effectively across diverse threat scenarios.

3) Antifragility in Autonomous Systems

Antifragility refers to the ability of a system not only to resist disruption but to improve under it [46]. In contrast to robustness, which ensures performance preservation, antifragile systems leverage perturbations as feedback for adaptation. Recent work in robotics and transportation systems explores antifragile design via uncertainty-aware control [47, 48], fragility spectrum quantification [49], and structural resilience in AAM networks [50]. Despite these advances, most approaches isolate antifragility from robustness rather than modeling them as points on a resilience continuum [51]. Additionally, the lack of a balancing feedback mechanism limits practical antifragility. In our approach, this feedback is achieved by switching among robust models trained under varying perturbation conditions, allowing the agent to improve its response under previously unseen attacks while preserving core safety objectives.

B. Novelty, Contribution and Impact

In this paper, we present a novel antifragility framework for UAV deconfliction in environments consisting of 3D obstacles, integrating adaptive switching between pre-trained adversarial action-robust RL policies and a standard pre-trained policy. First, we design action-robust RL policies that account for various perturbations in the policy space. To dynamically select the most appropriate policy in response to adversarial threats, we employ a discounted Thompson sampling (DTS) approach, modeling robust policies as multi-armed bandits (MAB). The switching mechanism is designed to minimize the value distribution shifts caused by adversarial attacks, which are generated using the Frank-Wolfe algorithm. The DTS-based switching strategy enables the system to select robust policies effectively in the presence of previously unseen

adversarial attacks. The key contributions of this work are as follows.

- **Antifragile Policy Switching Framework:** We propose a novel antifragile reinforcement learning framework for UAV deconfliction in 3D obstacle environments, combining an ensemble of action-robust policies with a Discounted Thompson Sampling (DTS)-based switching strategy. Robust policies are modeled as arms in a multi-armed bandit (MAB) setup, and selected adaptively based on value distributional shifts induced by adversarial attacks.
- **Theoretical Guarantees for Robust Adaptation:** We present formal regret analysis and convergence guarantees showing that DTS asymptotically selects the optimal robust policy under nonstationary, unseen adversarial perturbations. Additionally, we theoretically characterize antifragility as the agent's ability to improve performance under increasing distributional shifts via adaptive policy switching.
- **Empirical Validation in Adversarial UAV Scenarios:** We benchmark the proposed approach against existing robust RL methods, including adversarial and probabilistic training, under projected gradient descent (PGD) and hijack-induced spoofing attacks in complex 3D airspace environments. Our method consistently outperforms baselines in reward preservation and conflict avoidance.

Paper Organization: Section II elaborates on the RL and IFDS methodologies used for deconfliction in environments with 3D obstacles. Section E.II provides a comprehensive examination of action-based RL. In Section IV, the formulation of the robust policies as multi-armed bandits are considered, along with the respective Bernoulli rewards. Section V focuses on the optimality of the Bernoulli rewards with respect to the distribution shift considering the regret minimization problem, and the optimality of adaptation during test-time due to DTS sampler while inducing antifragility. A detailed analysis of the results, including a comparative assessment against robust algorithms based on benchmarks, is provided in Section VI. Finally, Section VII synthesizes the key findings and conclusions.

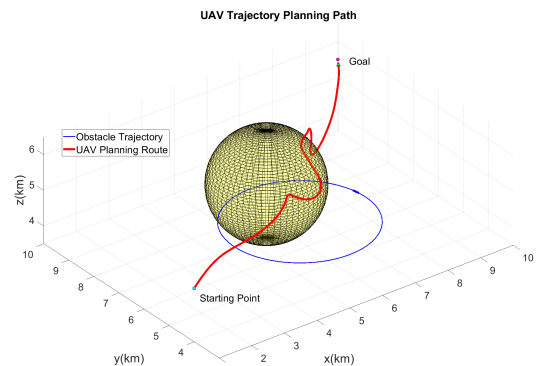


Fig. 1. The navigation environment for UAV against 3D dynamic obstacle with the trajectory computed using IFDS.

II. 3D UAV NAVIGATION: ENVIRONMENT AND AGENT DESCRIPTION

A. State Transition Model

The modelling environment is a tactical deconfliction problem as shown in Fig.1, where the UAV has to navigate from the starting point to the goal via a dynamic 3D obstacle. The resulting trajectory is computed by the interaction between the original flow field due to the target and the interfered flow field due to the obstacle(s). The initial flow field is designed to converge at the target destination where position vector \mathbf{P} , influences the velocity $u(\mathbf{P})$ of the UAV as:

$$u(\mathbf{P}) = - \left[\frac{C(x-x_d)}{\bar{d}(\mathbf{P}, \mathbf{P}_d)}, \frac{C(y-y_d)}{\bar{d}(\mathbf{P}, \mathbf{P}_d)}, \frac{C(z-z_d)}{\bar{d}(\mathbf{P}, \mathbf{P}_d)} \right]^T, \quad (1)$$

where C is the convergence speed and \bar{d} being the Euclidean distance between current position \mathbf{P} and the target position \mathbf{P}_d .

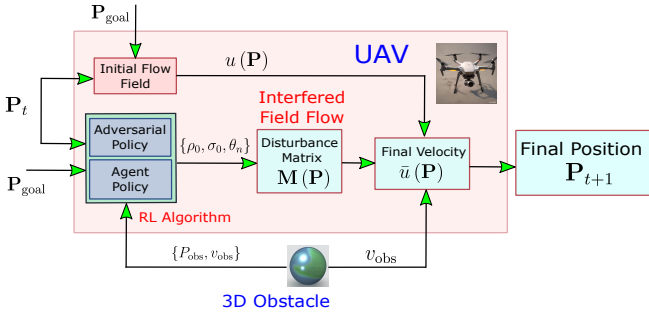


Fig. 2. The practical implementation of the RL algorithm for the UAV navigation, whose path is smoothed by IFDS.

However, the initial flow field is affected due to the presence of dynamic obstacles. The extent of the change can be captured using $\bar{M}(\mathbf{P})$ which is derived in Appendix A, which is dependant on the shape of the obstacles. The resulting synthetic disturbance flow field in the dynamic obstacle environment is provided as follows,

$$\bar{u}(\mathbf{P}) = \bar{M}(\mathbf{P})(u(\mathbf{P}) - v_{\text{obs}}(\mathbf{P})) + v_{\text{obs}}(\mathbf{P}). \quad (2)$$

For the point \mathbf{P}_t , on the path \mathbf{P}_{t+1} is obtained by integrating the disturbed flow field:

$$\mathbf{P}_{t+1} = \mathbf{P}_t + \bar{u}(\mathbf{P}_t) \Delta T. \quad (3)$$

In reality, the IFDS manifests itself in the modified actions after the output of the optimization agent action space (e.g., in the rotorcraft controllers) as per the implementation shown in Figure 2.

B. Reinforcement Learning Agent

The first step in defining the RL problem involves formulating the environment transition model given by the position update equation in (3), which accounts for both the initial and perturbed flow fields. The subsequent subsections will explain the state, action, and reward for the RL agent.

1) States

The ownship UAV, navigated by an RL agent, acquires data from the closest moving obstacles - potentially another UAV following a predefined trajectory - via ADS-B as part of the UTM infrastructure. This data includes the obstacle's position \mathbf{P}_{obs} and its velocity v_t^{obs} at time t . Consequently, the UAV considers its relative position to both the destination and the obstacle, as well as the obstacle's velocity, as input states. Hence, the agent state Φ_t at time t is given as:

$$\Phi_t = \left\{ \mathbf{P}_{\text{goal}} - \mathbf{P}_{\text{UAV}}, \mathbf{P}_{\text{obs}} - \mathbf{P}_{\text{UAV}}, v_t^{\text{obs}} \right\}. \quad (4)$$

2) Reward

The first reward mechanism R_1 is in the form of penalty signal if the planned navigation point \mathbf{P}_{t+1} is inside the dynamic obstacle, which is represented as:

$$R_1 = \frac{\|\mathbf{P}_{t+1} - \mathbf{O}_{\text{obs}}\|}{R_{\text{obs}}} \text{ if } \|\mathbf{P}_{t+1} - \mathbf{O}_{\text{obs}}\| \leq R_{\text{obs}}, \quad (5)$$

where \mathbf{O}_{obs} is considered the center of the obstacle ball, R_{obs} is considered its radius. In case the UAV planned path is not inside the dynamic obstacles, the reward mechanism aims to optimize the path length, which can be specified as:

$$R_2 = \begin{cases} -\frac{\|\mathbf{P}_{t+1} - \mathbf{P}_g\|}{\|v_{\text{obs}} - \mathbf{P}_g\|} & \text{if } \|\mathbf{P}_{t+1} - \mathbf{P}_g\| > \varepsilon, \\ -\frac{\|\mathbf{P}_{t+1} - \mathbf{P}_g\|}{\|v_{\text{obs}} - \mathbf{P}_g\|} + C_1 & \text{if } \|\mathbf{P}_{t+1} - \mathbf{P}_g\| \leq \varepsilon. \end{cases} \quad (6)$$

As described in (6), the deconfliction is achieved by prioritizing the shortest path to the target. However, this shortest path may bring the UAV closer to the obstacle surface. To address this risk, a threat zone is defined around the obstacle, where a penalty is imposed if the planned path intersects this zone.

$$R_3 = \frac{\|\mathbf{P}_{t+1} - \mathbf{O}_{\text{obs}} - (R_{\text{obs}} + r)\|}{R_{\text{obs}}} - C_2, \quad (7)$$

if $R_{\text{obs}} < \|\mathbf{P}_{t+1} - \mathbf{O}_{\text{obs}}\| < R_{\text{obs}} + r$.

As specified in (7) $r > 0$ is considered a threat area where C_2 is a positive constant. Hence, we can scale the above rewards R_1 , R_2 and R_3 as,

$$R_t(a_t | s_t) = \lambda_1 \cdot R_1 + \lambda_2 \cdot R_2 + \lambda_3 \cdot R_3. \quad (8)$$

where $\lambda_1, \lambda_2, \lambda_3 > 0$ is considered as a weighting factor.

3) Action

The parameters $\{\rho_0, \zeta_0, \vartheta_n\}$ for the IFDS as an action of the agent.

III. ACTION ROBUST REINFORCEMENT LEARNING

As illustrated in Figure 3, the schematic is shown to obtain a set of robust policies by varying the parameter α . The agent and adversarial policies, denoted as π_θ and μ_ω , respectively, generate action a_t based on a weighted combination: $(1 - \alpha_t) a_t^{\text{agent}}$ for the agent and αa_t^{adv} for the adversary. These actions determine the trajectory of navigation of a UAV in 3D obstacle environment. Upon executing an action a_t , the agent receives a reward r_t while transitioning to a new state Φ' . The agent's overall experience is stored as $e_t = \{\Phi_t, a_t, r_t, \Phi'_t\}$ in the replay buffer $\mathcal{D}_{\text{replay}}$. Subsequently, a batch of experiences

$\mathcal{D} = \{e_1, \dots, e_N\}$ is sampled from the replay buffer to compute the critic and the corresponding actor loss function.

To facilitate joint optimization of agent and adversarial policies under a common critic, a min-max objective is formulated. Stochastic gradient descent (SGD) updates are performed with added noise to prevent the Nash equilibrium solution from becoming trapped at saddle points. Once the agent is trained, the difference in entropy between the exploration and exploitation rewards, ΔH , is computed. If ΔH exceeds a predefined threshold, the training resumes with an updated value α . However, if ΔH falls below the threshold, the training is terminated, resulting in the final set of robust action policies.

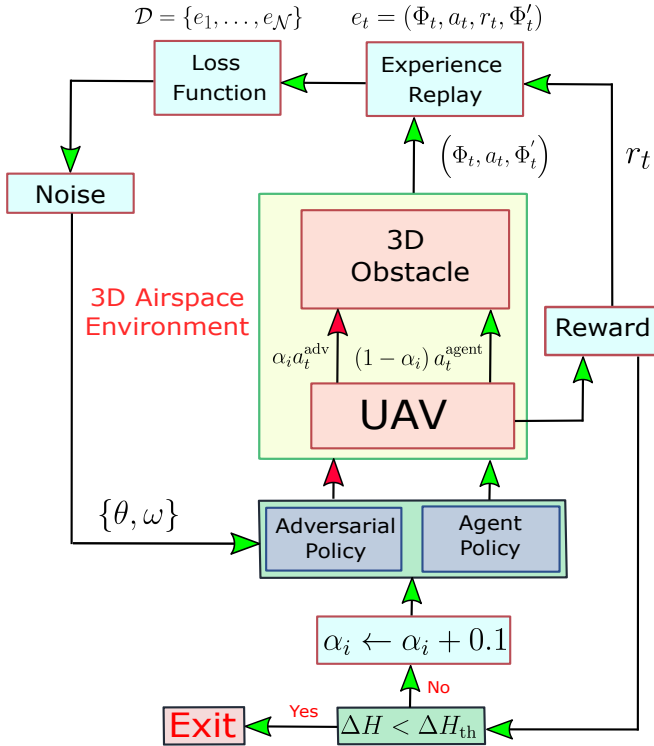


Fig. 3. The schematic to train the ensemble adversarial action robust DDPG for various α_i until the convergence is obtained in terms of entropy ΔH .

In the context of a vanilla RL, we define the Markov decision process (MDP) $\mathcal{M} := (\mathcal{S}, \mathcal{A}, T_1, \gamma, P_0, R_1)$, where \mathcal{S} and \mathcal{A} represent the state and action spaces, respectively. For addressing RL problems with continuous action spaces, we define it as $\mathcal{A} \in \mathbb{R}^d$. The transition dynamics is given by $T_1 : \mathcal{S} \times \mathcal{S} \times \mathcal{A} \rightarrow [0, 1]$ where $T_1(\Phi_t | \Phi_t, a_t)$ denotes the probability of reaching the state Φ_t' by taking the action a_t at the state Φ_t . $P_0 : \mathcal{S} \rightarrow [0, 1]$ represent the initial distribution on \mathcal{S} . γ is considered as the discount factor $R_1 : \mathcal{S} \times \mathcal{A} \rightarrow \mathbb{R}$ represents the reward of the environment after taking the action a_t .

However, to train agent and adversarial policies in a shared action space, a two-player zero-sum Markov game is used [42]. In this setting, both players simultaneously select an action and the reward is determined by the current state Φ_t and

the joint actions of the agent and adversarial policies, which influences the transition dynamics. The MDP models the game as $\mathcal{M}_2 = (\mathcal{S}, \mathcal{A}, \mathcal{A}', T_2, \gamma, R_2, P_0)$ where \mathcal{A} and \mathcal{A}' denote the action spaces available to the agent and the adversary. The state transition probability is given by $T_2 : \mathcal{S} \times \mathcal{A} \times \mathcal{A}' \times \mathcal{S} \rightarrow \mathbb{R}$ and $R_2 : \mathcal{S} \times \mathcal{A} \times \mathcal{A}' \rightarrow \mathbb{R}$ defines the reward for both players. Here, the agent's policy is represented by $\mu : \mathcal{S} \rightarrow \mathcal{A}$, while the adversary follows the policy $\nu : \mathcal{S} \times \mathcal{A}'$ within the environment \mathcal{M}_2 . At each time step t , the agent and the adversary select actions $a_t = \mu(\Phi_t)$ and $a_t' = \nu(\Phi_t)$, respectively. In the context of a zero-sum game, the agent receives a reward $r_t = R_2(\Phi_t, a_t, a_t')$, while the adversary receives a reward of $-r_t$. In the adversarial game, the following performance objective is considered for optimization.

$$J(\mu, \nu) = \mathbb{E} \left[\sum_{t=1}^{\infty} \gamma^{t-1} r_t \mid \mu, \nu, \mathcal{M}_2 \right], \quad (9)$$

where $\sum_{t=1}^{\infty} \gamma^{t-1} r_t$ is the random cumulative return. If we consider parameterized policies $\{\mu_\theta : \theta \in \Theta\}$ and $\{\nu_\omega : \omega \in \Omega\}$ for the agent and adversary policy respectively, the reward maximization objective is given as:

$$\max_{\theta \in \Theta} \min_{\omega \in \Omega} J(\mu_\theta, \nu_\omega). \quad (10)$$

The objective J in (10) is non-convex and non-concave with respect to both θ and ω . To address this, the analysis considers the set of all probability distributions over Θ and Ω aiming to identify the optimal distribution that solves the following objective:

$$\max_{p \in \mathcal{P}(\Theta)} \min_{q \in \mathcal{P}(\Omega)} f(p, q) := \mathbb{E}_{\theta \sim p} [\mathbb{E}_{\omega \sim q} [J(\mu_\theta, \nu_\omega)]]. \quad (11)$$

The objective defined in (11) can be solved using stochastic gradient Langevin dynamics as shown in Appendix ?? To determine the number of models in the ensemble set of agent and adversarial policies, entropy is employed as a metric. According to [52, 53], the goal to achieve robustness in RL is to minimize the maximum entropy of environmental states. With the increase in adversarial policy's contribution to the action space, we expect the entropy difference between the exploitation and exploration phases of learning to decrease. However, at higher levels of adversarial contribution, states may exhibit increased entropy, leading to greater randomness in episodic rewards. Let \mathbf{H}_{rand} represent the reward entropy during the exploration phase and \mathbf{H}_{opt} during the exploitation phase; then, the difference in entropy can be expressed as $\Delta \mathbf{H} = \mathbb{E} \left[\Delta \mathbf{H}_{\alpha_i}^{\text{rand}} - \max \left[\mathbf{H}_{\alpha_i}^{\text{opt}} \right] \right]$. As shown in Figure 3, $\Delta \mathbf{H}$ is used as a metric to find the required number of ensembles, where, if it goes below, ΔH_{th} then we do not consider the given model within the ensemble set. To determine the number of models in the ensemble set of agent and adversarial policies, entropy is employed as a metric. According to [52, 53], the goal to achieve robustness in RL is to minimize the maximum entropy of environmental states. With the increase in adversarial policy's contribution to the action space, we expect the entropy difference between the exploitation and exploration phases of learning to decrease. However, at higher levels of adversarial contribution, states may exhibit increased entropy, leading to greater randomness in episodic rewards. Let \mathbf{H}_{rand}

represent the reward entropy during the exploration phase and \mathbf{H}_{opt} during the exploitation phase; then, the difference in entropy can be expressed as $\Delta\mathbf{H} = \mathbb{E} \left[\Delta\mathbf{H}_{\alpha_i}^{\text{rand}} - \max \left[\mathbf{H}_{\alpha_i}^{\text{opt}} \right] \right]$. As shown in Figure 3, $\Delta\mathbf{H}$ is used as a metric to find the required number of ensembles, where, if it goes below, ΔH_{th} then we do not consider the given model within the ensemble set. The entire algorithm to obtain the ensemble of robust policies is shown in Algorithm 1.

IV. DISCOUNTED THOMPSON SAMPLING FOR SWITCHING ROBUST POLICIES

As illustrated in Figure 4, the antifragility framework employs a DTS-based mechanism to dynamically switch between robust policies in response to adversarial observations. Initially, adversarial observations, denoted as Φ_{adv} , are synthesized from the original observations Φ by incorporating the gradient sign of DDPG actor loss, $\nabla_{\Phi} \mathcal{L}_{\pi}$, with the maximum magnitude of the perturbation ε . Using the robust action policy, as described in the previous section, the corresponding adversarial action \mathbf{a}_{adv} is derived. Currently, actions \mathbf{a} are obtained from the original observations Φ using the deep deterministic policy gradient (DDPG) policy. To assess the impact of adversarial observations, the value distributions are obtained from trained critics, specifically $Q(\Phi, \mathbf{a})$ for vanilla DDPG and $Q_{\text{rob}}(\Phi_{\text{adv}}, \mathbf{a}_{\text{adv}})$ for action robust DDPG. The distributional shift is quantified using the Wasserstein distance between these value functions. Subsequently, the distributional shift is normalized with respect to the minimum distance in all robust value functions to compute the true probability p_{true} .

Given the robust model selected, the Bernoulli reward, which represents the likelihood, is calculated based on a Beta prior with parameters (a, b) , while updating the conjugate Beta posterior distribution. After a certain number of time steps, once the posterior update for the DTS is complete, the attack strength is increased by $\Delta\varepsilon$, resulting in a new set of probabilities, \mathbf{p}_{true} , thus addressing the nonstationary Bernoulli reward. Consequently, the DTS parameters (a, b) are updated with a discount factor η , which accounts for the temporal variations in \mathbf{p}_{true} . The methodology for generating adversarial observations using the Frank-Wolfe optimization technique is presented in the following subsection.

A. Adversarial Observations

In the context of antifragility, adaptation must take into account adversarial observations to ensure robustness. Given that the structure of the model is known, adversarial perturbations are formulated under a white-box attack framework. In this paper, a projection-free adversarial attack mechanism based on the Frank-Wolfe algorithm [54] is used. This approach leverages an iterative first-order white-box attack with momentum, which exhibits a convergence rate of $O(1/\sqrt{T})$, where T represents the number of steps. For a given state representation Φ , let $\mathcal{P}_{\mathcal{X}}(\Phi)$ denote the projection operation that maps the observation Φ to the constraint set \mathcal{X} at each iteration. In contrast to the projected gradient descent attack (PGD) [55], the Frank-Wolfe algorithm is inherently projection-free, as it instead relies on a linear minimization oracle (LMO) over the

constraint set \mathcal{X} at each iteration. The LMO is defined as follows,

$$\text{LMO} \in \arg \min_{\Phi_{\text{adv}} \in \mathcal{X}} \langle \Phi_{\text{adv}}, \nabla \mathcal{L}_{\pi}(\Phi) \rangle. \quad (12)$$

The LMO in (12) is seen as the minimization of the first-order Taylor expansion of \mathcal{L}_{π} at Φ :

$$\min_{\Phi_{\text{adv}} \in \mathcal{X}} \mathcal{L}_{\pi}(\Phi) + \langle \Phi_{\text{adv}} - \Phi, \nabla \mathcal{L}_{\pi}(\Phi) \rangle. \quad (13)$$

The minimization procedure to obtain an adversarial state in (13) can be implemented using the process shown in Algorithm 2. In the Frank-Wolfe algorithm, the linear minimization oracle (LMO) optimally solves a linear subproblem in the constraint set, \mathcal{X} , followed by a weighted averaging step with the previous iterate to compute the final update as shown in Algorithm 2. Compared to the PGD attack, the Frank-Wolfe approach is more conservative, as it eliminates the need for explicit projection steps, resulting in improved distortion characteristics.

B. Distributional Shift Due to Adversarial Observation

The shift in the value distribution caused by adversarial observations is quantified using the 1-Wasserstein norm, which is normally used to measure the distance between probability distributions. Let $\mathcal{P}(\mathbb{R}^d)$, denote the space of probability measures in \mathbb{R}^d with finite first moments. Given two probability measures, $\sqsupset, \sqsupset \in \mathcal{P}(\mathbb{R}^d)$, the 1-Wasserstein is defined as:

$$\mathcal{W}_1(\sqsupset, \sqsupset) = \inf_{t \in \Pi(\mu, \nu)} \mathbb{E}_{(x, y) \sim t} [\|x - y\|]. \quad (14)$$

Here $\Pi(\sqsupset, \sqsupset)$ represents the set of all joint distributions t with marginals \sqsupset and \sqsupset . $\|x - y\|$ represents the Euclidean norm in \mathbb{R}^d , and $\mathbb{E}_{(x, y) \sim t} [\|x - y\|]$ quantifies the cost of transporting mass from x to y . Similarly, if we consider a critic for vanilla DDPG be Q and for action robust critic as Q_{AR}^{α} , for which we can define the value distribution $Z(\Phi)$ and $Z_{\text{AR}}^{\alpha}(\Phi_{\text{adv}})$ follows:

$$\begin{aligned} Z(\Phi) &= Q_{\text{DDPG}}(\Phi, \pi(\Phi)), \\ Z_{\text{AR}}^{\alpha}(\Phi) &= Q_{\text{AR}}^{\alpha}(\Phi_{\text{adv}}, \alpha \cdot \pi_{\text{adv}}(\Phi) + (1 - \alpha) \cdot \pi_{\text{agent}}). \end{aligned} \quad (15)$$

We define the distribution shift d_{ε}^{α} due to adversarial observation Φ_{adv} due to adversarial attack of intensity ε as,

$$d_{\varepsilon}^{\alpha} = \inf_{\gamma \in \Pi(Z, Z_{\text{AR}}^{\alpha})} \mathbb{E}_{(x, y) \sim \gamma} [\|x - y\|]. \quad (16)$$

Similarly for DDPG policy, π_{DDPG} , we define the value distribution at adversarial observation Φ_{adv} as,

$$Z_{\text{adv}} = Q(\Phi_{\text{adv}}, \pi_{\text{DDPG}}(\Phi_{\text{adv}})). \quad (17)$$

The value distribution shift for the DDPG due to adversarial observation Φ_{adv} of magnitude, ε i.e. d_{ε} is defined as,

$$d_{\varepsilon} = \inf_{t \in \Pi(Z, Z_{\text{adv}})} \mathbb{E}_{(x, y) \sim t} [\|x - y\|]. \quad (18)$$

Thus, for an adversarial observation with a given perturbation magnitude ε , the resulting distribution shift can be analyzed for both the standard DDPG and action-robust policies under varying levels of policy perturbation α as follows:

$$\mathbf{d} = \{d_{\varepsilon}^0, d_{\varepsilon}^{\alpha_1}, \dots, d_{\varepsilon}^{\alpha_n}\}. \quad (19)$$

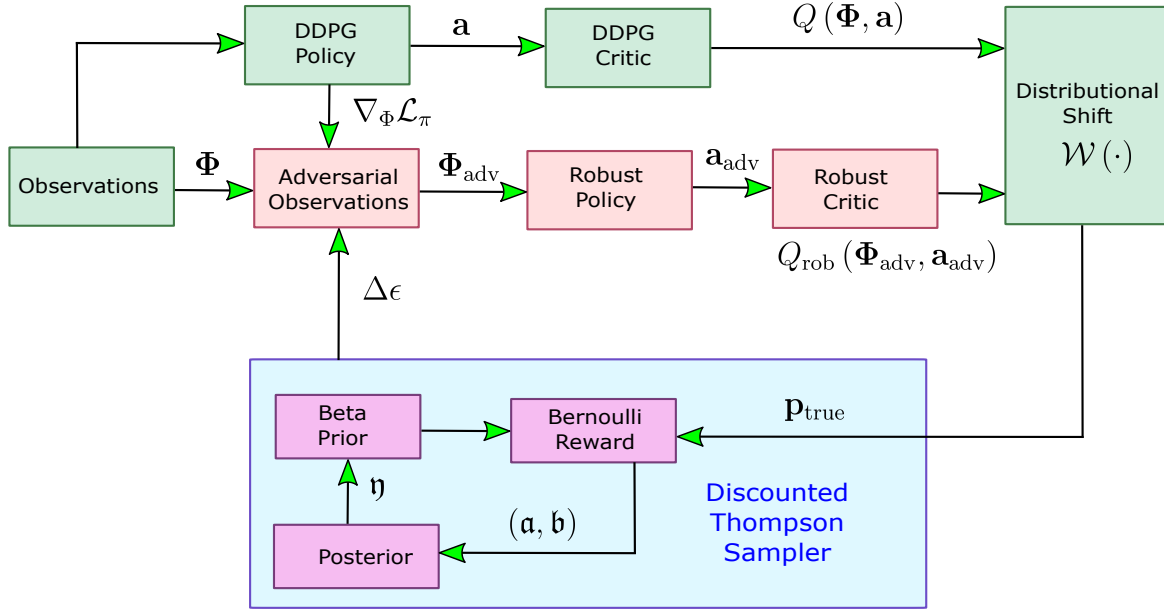


Fig. 4. Discounted Thompson sampling (DTS) technique to select the for antifragility.

However, to incorporate Bernoulli rewards for DTS, the distribution shifts must be transformed into equivalent Bernoulli-distributed rewards. Let $d_{\min} = \min(\mathbf{d})$, denote the minimum distribution shift. Using this, we can define the corresponding parameter for the Bernoulli rewards as follows:

$$\mathbf{p}_{\text{true}} = \left\{ \frac{k_{\text{mult}} \cdot d_{\min}}{d_{\epsilon}^0}, \frac{k_{\text{mult}} \cdot d_{\min}}{d_{\epsilon}^{\alpha_1}}, \dots, \frac{k_{\text{mult}} \cdot d_{\min}}{d_{\epsilon}^{\alpha_n}} \right\}. \quad (20)$$

According to (20), a lower value of d_{ϵ}^{α} for a given robust model indicates a smaller shift in the state-action value distribution under an adversarial attack of magnitude ϵ . Consequently, a higher value p_{true} for a specific model enhances its likelihood of successful deployment in adversarial settings.

C. Discounted Thompson Sampling for Minimum Distribution Shift

Let $\mathcal{K} = \{\pi_0, \pi_1, \dots, \pi_n\}$ represent the set of robust policy networks as multi-armed bandits (MAB) available to counter an adversarial observation. Given a finite time horizon T , the DTS must select a policy network $\pi_k \in \mathcal{K}$ at each time step $t \in \{1, \dots, T\}$. Let $X_{k,t}$ denote the reward obtained by employing the k -th robust policy at time t . Consequently, the instantaneous reward $X_{k,t}$ follows a Bernoulli distribution with an expected value of $\check{\mu}_{k,t} = \mathbb{E}[X_{k,t}]$. Therefore, the optimal policy at any given time t is the one that maximizes the expected reward, expressed as $\check{\mu}_t^* = \max_{k \in \mathcal{K}} \{\check{\mu}_{k,t}\}$.

In non-stationary environments, the expected Bernoulli rewards evolve over time, either following a gradual trend or undergoing abrupt changes. The sequence of rewards for a specific policy π_k is denoted by $\check{\mu}^k = \{\check{\mu}_{k,t}\}_{t=1}^T$, while the general sequence of rewards across all policies is represented as $\check{\mu} = \{\check{\mu}^k\}_{k \in \mathcal{K}}$. If we consider \mathcal{P} to be the family of admissible antifragile policies for DTS, let $\varkappa \in \mathcal{P}$ represent a candidate policy responsible for selecting an appropriate robust policy in response to adversarial observations. At each time

step t , the policy \varkappa chooses the robust policy I_t^{\varkappa} based on an initial prior U and past switching decisions $\{X_{I_t^{\varkappa}, n}\}_{n=1}^{t-1}$. Hence, the DTS switching policy \varkappa_t at time t is given by,

$$\varkappa_t = \begin{cases} \varkappa_1(U) & ; t = 1 \\ \varkappa_t(U, X_{I_{\varkappa_1, 1}}, \dots, X_{I_{\varkappa_{t-1}, t-1}}) & ; t \geq 2 \end{cases}. \quad (21)$$

Thompson Sampling (TS) [56] operates by maintaining a prior distribution over the success probabilities of each Bernoulli-based robust policy and sampling from this prior to determine which robust model to deploy. The prior distribution is typically modeled as a Beta distribution $\mathfrak{B}(a, b)$, with the parameters $\{a, b\}$ updated based on the Bernoulli rewards obtained from the deployment of the robust model against adversarial observation.

In DTS [57], the central concept is to adjust the algorithm to increase the variance of the prior distribution for unexplored robust models, thus improving the probability of deploying these models in response to adversarial observations. Consider a_0 and b_0 , denote the initial values of the parameters for the Beta prior distributions, and \mathfrak{S}_k and \mathfrak{F}_k represent the parameters of the posterior Beta distribution, which are discounted before being updated. Consequently, the update equation for $\{\mathfrak{S}, \mathfrak{F}\}$ can be expressed as:

$$\begin{aligned} \mathbb{E}\mathfrak{S}_{k,t+1} &= \eta \mathbb{E}\mathfrak{S}_{k,t} + \check{\mu}_{k,t} \mathbb{P}(I_t^{\varkappa} = k), \\ \mathbb{E}\mathfrak{F}_{k,t+1} &= \eta \mathbb{E}\mathfrak{F}_{k,t} + (1 - \check{\mu}_{k,t}) \mathbb{P}(I_t^{\varkappa} = k). \end{aligned} \quad (22)$$

where, $\mathbb{P}(I_t^{\varkappa} = k)$ is the probability of selecting the robust model k at instant t with the existing Bernoulli reward history $\{\tau_{I_t^{\varkappa}, n}\}_{n=1}^{t-1}$. If we neglect the effect of a_0 and b_0 , for the robust model not deployed at the instant, we consider the posterior mean as,

$$\check{\mu}_{k,t+1} = \frac{\mathfrak{S}_{k,t+1}}{\mathfrak{S}_{k,t+1} + \mathfrak{F}_{k,t+1}} = \frac{\eta \cdot \mathfrak{S}_{k,t}}{\eta \cdot \mathfrak{S}_{k,t} + \eta \cdot \mathfrak{F}_{k,t}} = \check{\mu}_{k,t}. \quad (23)$$

We can write the variance using (22) as,

$$\check{\sigma}_{k,t+1}^2 = \frac{\mathfrak{S}_{k,t+1} \cdot \tilde{\mathfrak{F}}_{k,t+1}}{(\mathfrak{S}_{k,t+1} + \tilde{\mathfrak{F}}_{k,t+1})^2 (\mathfrak{S}_{k,t+1} + \tilde{\mathfrak{F}}_{k,t+1} + 1)}, \quad (24)$$

$$= \frac{\check{\mu}_{k,t}(1 - \check{\mu}_{k,t})}{\eta \cdot \mathfrak{S}_{k,t} + \eta \cdot \tilde{\mathfrak{F}}_{k,t} + 1} \geq \frac{\check{\mu}_{k,t}(1 - \check{\mu}_{k,t})}{\mathfrak{S}_{k,t} + \tilde{\mathfrak{F}}_{k,t} + 1}. \quad (25)$$

We observe in (24) that the discounting increases the variance of the prior distribution, which in-turn help tackle the non-stationarity of the rewards.

V. THEORETICAL ANALYSIS

In this section we will theoretically prove that DTS based switching of robust policies, help the algorithm deal with adaptation against unseen attacks and induce antifragility.

A. Regret Minimization

Before we consider the regret minimization analysis while deploying the optimal robust policy, we consider the following assumption.

Assumption 1 *The expected return of any policy π_k is Lipschitz-continuous in the Wasserstein distance between clean and adversarial value distributions:*

$$\left| \mathbb{E}[R(\pi_k; \Phi_t^{adv})] - \mathbb{E}[R(\pi_0; \Phi_t)] \right| \leq L \cdot d_k^{(t)}, \quad (26)$$

where $L > 0$ is a constant

Above assumption takes into account the engineering realism of non-sudden shift in the reward due to adversarial states. Let us define a proxy reward to assess robustness, similar to (20), which assigns higher reward to policies which exhibits smaller value shifts under perturbation.

$$r_k^{(t)} := \frac{d_{\min}^{(t)}}{d_k^{(t)}} \in (0, 1], \quad \text{with } d_{\min}^{(t)} := \min_j d_j^{(t)}. \quad (27)$$

Hence if we consider $\pi_{k^*} := \arg \min_k d_k^{(t)}$ as the optimal policy for DTS with minimal shift under perturbation, the instantaneous regret is given by:

$$\mu_{k^*} - \mu_{k_t} \leq L \cdot \left(d_{k_t}^{(t)} - d_{\min}^{(t)} \right) = L \cdot \left(\frac{1}{r_{k_t}^{(t)}} - 1 \right) d_{\min}^{(t)}. \quad (28)$$

As we sum over a time horizon T , hence we obtain the overall regret $\mathcal{R}(T)$,

$$\mathcal{R}(T) := \sum_{t=1}^T (\mu_{k^*} - \mu_{k_t}^{(t)}) \leq L \sum_{t=1}^T \left(\frac{1}{r_{k_t}^{(t)}} - 1 \right) d_{\min}^{(t)}. \quad (29)$$

It shows that minimizing the regret is equivalent to selecting the DTS policy with the minimal value shift which justifies the use of $d_k^{(t)}$ in (19) as a robustness metric.

As shown in [57], DTS achieves sublinear regret in multi-armed bandit problems with M changepoints, shown as

$$\mathbb{E}[\mathcal{R}(T)] \leq O\left(\sqrt{KMT \log T}\right). \quad (30)$$

Substituting into our bound, we get,

$$\mathbb{E}\left[\sum_{t=1}^T \left(\frac{1}{r_{k_t}^{(t)}} - 1 \right) d_{\min}^{(t)}\right] \leq \frac{1}{L} \cdot O\left(\sqrt{KMT \log T}\right), \quad (31)$$

where κ_t is the policy selected by DTS at time t . As the regret is minimized with respect to non-stationary adversarial attacks, now we see the nature of the algorithm against unseen adversarial attacks.

B. Adaption to Unseen Adversarial Attacks

Theorem 1 (Adaptive Robustness of DTS) *Let*

$\mathcal{K} = \{\pi_1, \dots, \pi_K\}$ *be a finite set of robust policies, each associated with a reward proxy $r_k^{(t)} := \frac{d_{\min}^{(t)}}{d_k^{(t)}} \in (0, 1]$,*

where $d_k^{(t)}$ is the Wasserstein-1 distance between the clean and adversarial value distributions under policy π_k at time t . We assume the Lipschitz nature of the reward function, and consider a unique optimal policy under each stationary segment. Then, the DTS policy selector κ_t converges in probability to selecting the optimal policy k^ within each stationary segment. Then we can consider,*

$$\lim_{t \rightarrow \infty} \mathbb{P}(\kappa_t = k^*) = 1.$$

Proof: Consider a stationary interval $I = [\tau_s, \tau_{s+1})$ during which the adversarial perturbation remains fixed, and the reward proxies $r_k^{(t)}$ are i.i.d. samples from a Bernoulli distribution with mean μ_k for each policy π_k . as we know the DTS maintains Beta posteriors over $r_k^{(t)}$:

$$\tilde{r}_k^{(t)} \sim \text{Beta}(S_k^{(t)} + a_0, F_k^{(t)} + b_0).$$

Here a_0, b_0 are the hyperparameter for the prior. Because the updates use discounted sufficient statistics, we can consider as per [57],

$$S_k^{(t)} = \sum_{i=1}^t \gamma^{t-i} r_k^{(i)}, \quad F_k^{(t)} = \sum_{i=1}^t \gamma^{t-i} (1 - r_k^{(i)}).$$

which gives a geometrically weighted moving average of the observed rewards. From the standard concentration inequalities [57], the posterior mean $\mathbb{E}[\tilde{r}_k^{(t)}]$ converges to the true reward mean μ_k as $t \rightarrow \infty$, with posterior variance decaying as $O((1 - \gamma)^2)$. Let us consider $k^* = \arg \max_k \mu_k$. The probability that DTS selects a suboptimal policy $j \neq k^*$ is:

$$\mathbb{P}(\tilde{r}_j^{(t)} > \tilde{r}_{k^*}^{(t)}).$$

Using concentration bounds for Beta-Binomial tail bounds [58], this probability decays exponentially:

$$\mathbb{P}(\tilde{r}_j^{(t)} > \tilde{r}_{k^*}^{(t)}) \leq \exp\left(-\frac{(\mu_{k^*} - \mu_j)^2}{C(1 - \gamma)^2}\right),$$

for a constant C depending on the reward range and prior. For each of the M change points in the adversarial distribution, a new stationary segment with a different optimal policy may emerge. Provided each segment is sufficiently long, DTS will adapt its sampling distribution by concentrating its posterior on the new k^* in each segment. Let $\Delta_s = \min_{j \neq k_s^*} (\mu_{k_s^*} - \mu_j)$ be the minimum reward gap in the segment where it is considered stationary, the regret is bounded by $O\left(\frac{K}{\Delta_s^2} \log T\right)$ and the total regret over all segment satisfies:

$$\mathbb{E}[\mathcal{R}(T)] \leq O\left(\sqrt{KMT \log T}\right). \quad (32)$$

Hence we can conclude that the policy with the minimal value distribution shift yields the highest proxy reward $r_k^{(t)}$ and the DTS posterior concentrates on the arms with the highest mean, which follows the following results.

$$\lim_{t \rightarrow \infty} \mathbb{P}(\kappa_t = \arg \min_k d_k^{(t)}) = 1$$

Remark 1 (Adaptation to Unseen Adversarial Attacks)

Theorem 1 implies that the DTS mechanism enables robust policy adaptation even in the presence of previously unseen or out-of-distribution (OOD) adversarial perturbations. Although the policy ensemble $\mathcal{P} = \{\pi_{\alpha_1}, \dots, \pi_{\alpha_K}\}$ is trained only on a discrete set of known adversarial intensities $\{\alpha_k\}$, DTS does not require explicit knowledge of the true test-time perturbation $\varepsilon_t \notin \{\alpha_1, \dots, \alpha_K\}$. Instead, DTS relies on online estimates of the value distribution shift $d_k^{(t)}$ as a proxy for robustness. As long as one policy in \mathcal{P} exhibits relatively low Wasserstein shift under the unseen attack (i.e., approximates the behavior needed to withstand ε_t), its reward proxy $r_k^{(t)} = d_{\min}^{(t)}/d_k^{(t)}$ will dominate over time. Due to posterior concentration, DTS will asymptotically prefer this policy, allowing the agent to adapt dynamically to new adversarial conditions without retraining. This property ensures that the agent is not merely robust, but adaptive to distributional shifts caused by novel adversarial strategies.

As per Theorem 1, DTS enables online selection of the policy that minimizes the distributional shift of the value function under unknown, time-varying, and even unseen adversarial attacks. Now we link the analysis, to how it makes the overall system antifragile.

C. Antifragile Behaviour

Definition 1 A RL system is said to exhibit antifragility under adversarial observation perturbations if, in response to increased perturbation intensity or out-of-distribution (OOD) attacks, the system adaptively improves its expected performance (reward) over time by leveraging the variability to refine its policy selection mechanism.

Now we based on the above definition, we move on to the theorem where we prove that the policy improvement under DTS makes the whole RL antifragile against unseen attacks.

Theorem 2 (Antifragile Policy Improvement) Let

$\mathcal{P} = \{\pi_{\alpha_1}, \dots, \pi_{\alpha_K}\}$ be a finite set of robust policies trained under adversarial intensities $\alpha_k \in [0, 1]$. Let κ_t denote the policy selected at time t by the DTS-based switching mechanism under an adversarial perturbation $\varepsilon_t \notin \{\alpha_1, \dots, \alpha_K\}$, i.e., an unseen attack. We consider the value shift satisfies the Lipschitz robustness assumption as in (1), with the reward proxy defined in (27) and DTS maintains a discounted Beta posterior as in (22). Then, under slowly evolving or piecewise-constant perturbation intensity ε_t , the expected reward of the selected policy improves over time:

$$\lim_{t \rightarrow \infty} \frac{d}{dt} \mathbb{E}[R(\pi_{\kappa_t}; \Phi_t^{\text{adv}})] > 0. \quad (33)$$

Thus, the system exhibits antifragile behavior by improving performance in response to previously unseen adversarial conditions.

Proof: By Theorem 1, the DTS switching strategy converges in probability to selecting the policy that minimizes the value distributional shift:

$$\lim_{t \rightarrow \infty} \mathbb{P}(\kappa_t = \arg \min_k d_k^{(t)}) = 1. \quad (34)$$

Let $k^* := \arg \min_k d_k^{(t)}$ denote the optimal policy under the current (unseen) perturbation. Since DTS samples utilizes the optimal policy k^* , and $r_k^{(t)} = d_{\min}^{(t)}/d_k^{(t)}$, we have:

$$\lim_{t \rightarrow \infty} r_{\kappa_t}^{(t)} \rightarrow 1 \Rightarrow \lim_{t \rightarrow \infty} d_{\kappa_t}^{(t)} \rightarrow d_{\min}^{(t)}. \quad (35)$$

By the Lipschitz assumption:

$$\mathbb{E}[R(\pi_{\kappa_t}; \Phi_t^{\text{adv}})] \geq \mathbb{E}[R(\pi_{k^*}; \Phi_t)] - L \cdot d_{\kappa_t}^{(t)}. \quad (36)$$

Differentiating both sides w.r.t. t , we get:

$$\frac{d}{dt} \mathbb{E}[R(\pi_{\kappa_t}; \Phi_t^{\text{adv}})] \geq -L \cdot \frac{d}{dt} d_{\kappa_t}^{(t)}. \quad (37)$$

As DTS converges to the optimal robust policy, $d_{\kappa_t}^{(t)}$ decreases over time:

$$\frac{d}{dt} d_{\kappa_t}^{(t)} < 0 \Rightarrow \frac{d}{dt} \mathbb{E}[R(\pi_{\kappa_t}; \Phi_t^{\text{adv}})] > 0. \quad (38)$$

Even though ε_t was not seen during training, the DTS mechanism adapts using value shift observations alone. Thus, it can identify and exploit the best available robust policy without retraining. This ability to *improve under perturbation* characterizes antifragility. Detailed algorithm for DTS algorithm is provided in Appendix 3.

VI. RESULTS AND DISCUSSIONS

A. Numerical Implementation

The software implementation of the DDPG algorithm, used for the deconfliction of UAV navigation in the environment consisting of dynamic 3D obstacles, has been considered as per [59]. During the training phase, the initial position of the UAV was randomly considered with a mean around (0, 2, 5) and a variance between 0 and 1, while the target destination was fixed at (10, 10, 5.5). Kinematic constraints, including a maximum ascent angle of $5\pi/9$ and a maximum descent angle of $-15\pi/36$, were applied when updating the UAV position. In addition, a protection radius of 1.5 units was enforced around the UAV. The dynamic obstacle used in training was restricted to follow a predefined path along the x-y plane, with its trajectory given by the following equation:

$$\begin{aligned} \mathbf{x}_{\text{obs}}(t) &= \mathbf{x}_{\text{obs}}(t-1) + 2 \cos(t), \\ \mathbf{y}_{\text{obs}}(t) &= \mathbf{y}_{\text{obs}}(t-1) + 2 \sin(t). \end{aligned} \quad (39)$$

The reward function calculates the conflict penalty by augmenting the UAV's radius with an additional buffer of 0.4 units. The vanilla agent and the adversarial action robust models in the ensemble were trained considering a single dynamic obstacle. The action robust RL model was trained according

TABLE I
ADVERSARIAL ACTION ROBUST RL PARAMETERS

Parameter	Value
Exploration Episodes	30
Replay buffer size	1e6
Minibatch size	128
Discount factor	0.99
Target network soft update rate	0.01
Agent and adversary network learning rate	0.01
Agent and adversary network momentum	0.9
Adversary noise parameter	0.1
Weight decay	5e-4
Critic learning rate	1e-3
Neural network optimizer	Adam
Exploration noise	$\mathcal{N}(0.05, 0.02)$
Maximum steps per episode	500
Total number of episodes	200
Total neural network layers	3
Robustness update rate (β)	0.9
Number of neurons in each layer	128
Number of dynamic obstacles in testing scenario	4

to the Algorithm 1, using the parameters specified in Table I. In obtaining the DTS for switching between robust policies, the sampler is initially trained with a fixed value of p_{true} over 800 time steps. Subsequently, p_{true} is updated by increasing ϵ by 0.5, as shown in Figure 4. The discounting parameter for updating the posterior Beta distribution is considered to be 0.8.

B. Training Results

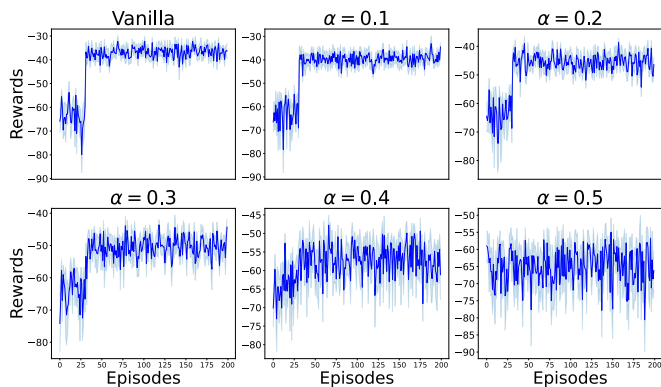


Fig. 5. Convergence plot for vanilla DDPG and adversarial action robust DDPG for various α .

The training results, based on the cumulative reward for the episode, are illustrated in Figure 5. The action robust RL model for adversarial actions was trained using varying proportions of adversarial influence in the action space, denoted as $\alpha = \{0.1, 0.2, 0.3, 0.4\}$. As shown in Figure 5, increasing α leads to greater uncertainty in the converged rewards, as reflected in the widening uncertainty bands. This trend is further confirmed by the mean entropy difference ΔH in Figure 6, where the gap between exploration and exploitation rewards decreases linearly with increasing α . To defend against evasion attacks during testing, it is crucial to train models with a less convex loss landscape. However, as the landscape of loss flattens, greater randomness is introduced

into the policy space, contributing to increased uncertainty in the final rewards.

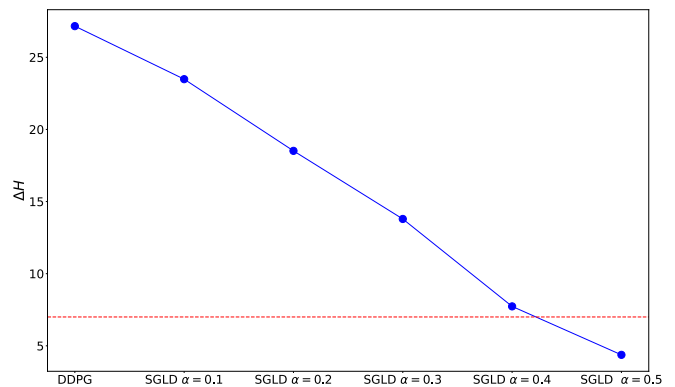


Fig. 6. The difference in the entropy obtained from the rewards obtained from exploration and exploitation phase for RL training for vanilla DDPG and adversarial action robust DDPG for various α .

C. Distribution Shift against Adversarial Attacks

Once robust action policies are established with $\alpha = \{0.1, 0.2, 0.3, 0.4\}$, we analyze how the state action value distribution of these robust models, along with the standard DDPG model, responds to adversarial perturbations. Adversarial observations are generated using the Frank-Wolfe optimization algorithm as stated in Algorithm 2, and the resulting value distributional shifts are depicted in Figure 7. Specifically, we compare value distributions under both benign conditions (no adversarial attack) and adversarial conditions where the attack magnitude is set to $\epsilon = 2.5$. A detailed distributional analysis

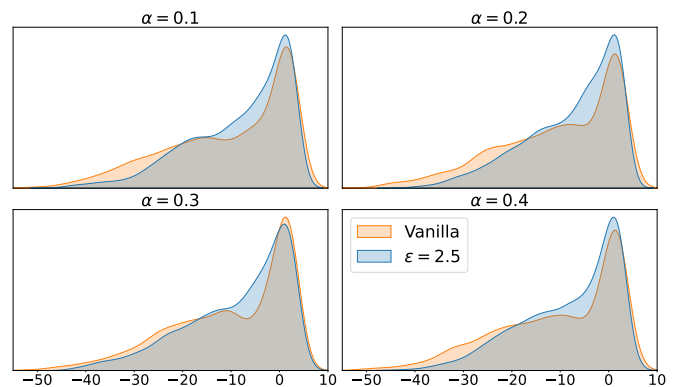


Fig. 7. The distribution shift for the critic values for the action robust RL with $\alpha = \{0.1, 0.2, 0.3, 0.4\}$ under normal operations and Frank Wolfe adversarial attack with $\epsilon = 2.5$.

reveals that the shift in the state-action value distribution, i.e. $\mathbf{d}_\epsilon^\alpha$, exhibits a linear increase with increasing ϵ in all models. In particular, for $\alpha = 0.3$, the magnitude of the distributional shift remains lower compared to other robust models. This trend is evident in Figure 7, where the mode of distribution of $\alpha = 0.3$ is closely aligned with that of the standard DDPG model, in contrast to other robust policies.

Next, we examine the behavior of \mathbf{p}_{true} that normalizes the distribution shift \mathbf{d}_ϵ according to (20). The multiplicative

factor k_{mult} that ensures a probability of 10% of selecting non-optimal models during deployment. A distinct variation in p_{true} is observed between low and high values of ϵ . Specifically, for $\alpha = 0.3$, p_{true} is the highest compared to DDPG and other robust action models. However, at $\epsilon = 1.0$, p_{true} is maximized for $\alpha = 0.2$, reinforcing the rationale behind employing DTS sampler instead of standard TS. A sharp transition in Bernoulli rewards is also expected between $\epsilon = 0.5$ and $\epsilon = 1.0$. Furthermore, as ϵ increases from 1.5 to 2.5, the relative decline in p_{true} amongst the action robust models diminishes, with $\alpha = 0.3$ consistently yielding the highest value of p_{true} . These findings suggest that the DTS should be trained to switch amongst the action robust models at a higher frequency to mitigate the impact of adversarially induced distributional shifts. Consequently, we progressively

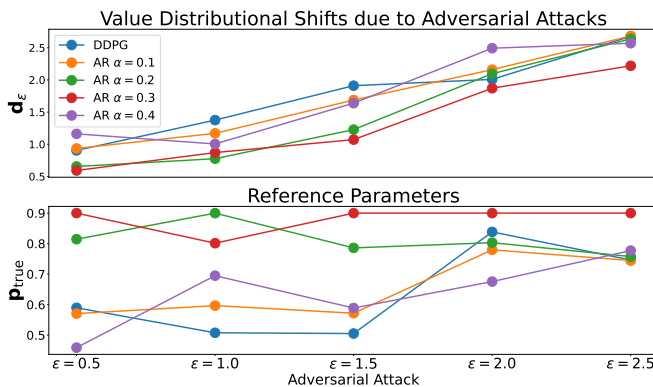


Fig. 8. a) The Wasserstein distance comparison between the critic values of vanilla DDPG and various action-robust DDPG formulations under incremental adversarial attacks. (b) The distributional shift induced by adversarial attacks, represented through the parameters of the Bernoulli distribution used for sampling.

train the DTS sampler using the p_{true} values that correspond to varying $\epsilon \in [0.5, 2.5]$, with a critical shift at $\epsilon = 1.0$, as illustrated in Figure 4. Additionally, for ablation studies, alternative sampling strategies such as undiscounted TS [56], epsilon-greedy (EPS) [60], and upper confidence bound (UCB) [61] have been evaluated. Although no significant differences are observed in overall rewards, the DTS algorithm exhibits superior safety performance in testing environments containing multiple dynamic obstacles, as illustrated in Figure 9 for $\epsilon = \{2.0, 2.5\}$.

D. Results against PGD Adversarial Attack

We further examine navigation performance under adversarial attacks, specifically considering a Projected Gradient Descent (PGD) attack with $N_{\text{steps}} = 50$. In practical scenarios, such attacks require knowledge of the policy network governing the navigation of the UAV. This policy can be inferred using generalized adversarial imitation learning [62] by exploiting unencrypted ADS-B data exchanges, which contain position and velocity information for both the UAV and dynamic obstacles. Using the extracted policy, an adversary can craft stealthy perturbations of a given magnitude ϵ . The resulting test rewards, depicted in Figure 10, correspond to the initial randomized conditions between episodes.

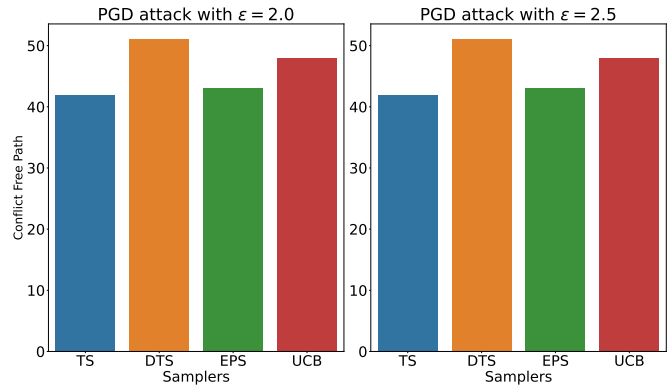


Fig. 9. The number of conflict-free paths generated by the antifragile algorithm over 100 episodes while comparing different sampling strategies. PGD adversarial attacks were applied at (a) $\epsilon = 2.0$ (b) $\epsilon = 2.5$.

The antifragile algorithm that uses the DTS sampler demonstrates superior performance, achieving higher testing rewards compared to the baseline algorithms. Furthermore, the variance in rewards is lower for the DTS-based approach, indicating increased stability. Safety performance is assessed by analyzing both the total number of conflicts and the proportion of conflict-free trajectories in the testing environment in Figures 11 and 12. The DTS algorithm significantly outperforms the robust and vanilla standard RL models in minimizing conflicts. However, while DTS marginally surpasses adversarial learning methods in overall performance, the latter exhibits a lower variance in conflict occurrences. Despite this, Figure 10 reveals that adversarial learning achieves lower overall rewards than the DTS-based method. This suggests that while adversarial learning improves collision safety, it does so at the expense of efficient path planning, thereby increasing vulnerability to alternative forms of attack.

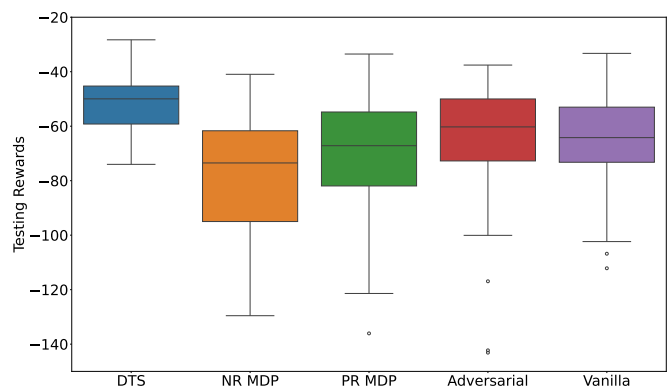


Fig. 10. The rewards obtained over 100 testing episodes in a multi-obstacle environment when evaluating the DTS-based antifragile algorithm against PGD adversarial attacks, in comparison to other robust RL techniques and vanilla DDPG.

E. Results against Spoofing Attacks for Hijacking

A separate analysis considers a different adversarial strategy, in which the position of the UAV is spoofed to facilitate hijacking [63]. This attack is commonly used to manipu-

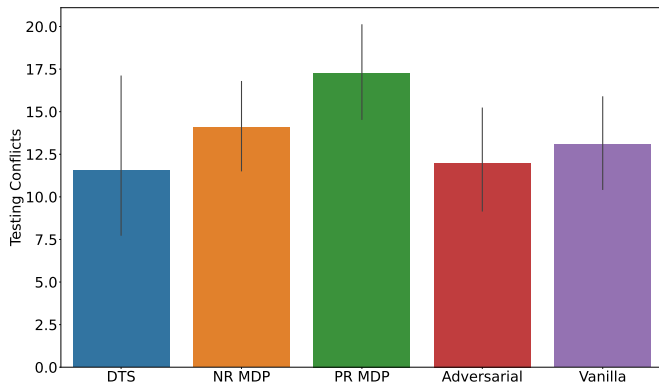


Fig. 11. The total number of conflicts encountered during UAV navigation under PGD adversarial attacks in a multi-obstacle environment, comparing the DTS-based antifragile algorithm with other robust RL techniques and vanilla DDPG over 100 episodes.

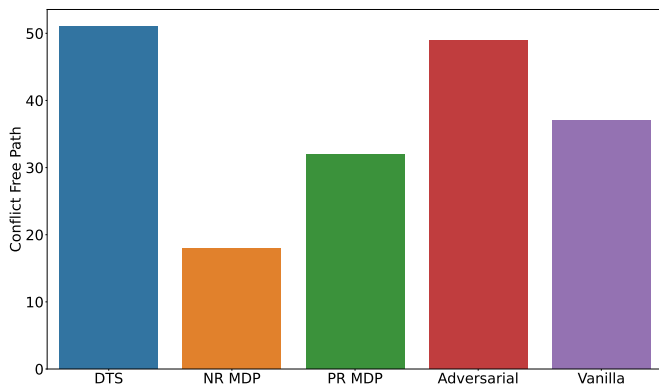


Fig. 12. The total number of conflict-free paths generated during UAV navigation under PGD adversarial attacks in a multi-obstacle environment, comparing the DTS-based antifragile algorithm with other robust RL techniques and vanilla DDPG over 100 episodes.

late position inputs, forcing UAVs to elongate flight paths through specific airspace zones, increasing exposure to hijacking attempts. To simulate this, the position of the UAV in each time step is perturbed with a uniform random bias $\mathcal{U}(0.04, 0.06)$. The objective is to determine whether the UAV deviates significantly from its intended trajectory. This scenario exemplifies antifragility, in which the algorithm is explicitly trained against adversarial disturbances to adapt to previously unseen attack patterns. As illustrated in Figure 13, the DTS-based antifragile algorithm maintains an optimal trajectory with minimal deviation, unlike alternative methods that exhibit excessive compensation in response to adversarial perturbations. Specifically, the rewards for NR-MDP and PR-MDP are notably lower due to their reliance on fixed countermeasures. In contrast, the adaptive nature of the DTS sampler, trained in non-stationary Bernoulli rewards, enables effective path planning while mitigating deviations induced by spoofing attacks. Consequently, the proposed approach ensures improved resilience against hijacking attempts while preserving efficient navigation.

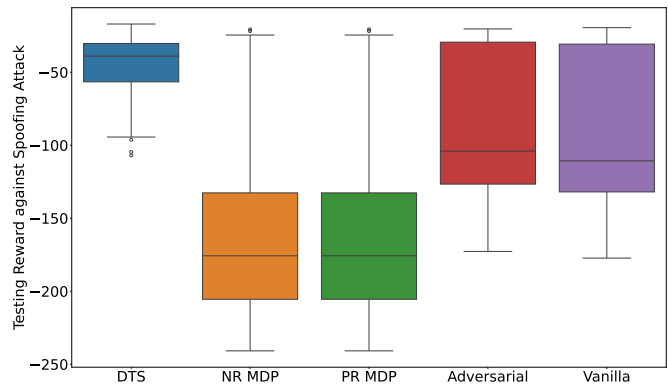


Fig. 13. The rewards obtained over 100 testing episodes when evaluating the antifragile algorithm with a DTS sampler against other robust RL techniques and vanilla DDPG under spoofing attacks.

VII. CONCLUSIONS

In this study, an antifragile reinforcement learning (RL) framework has been developed, employing a mechanism for switching between robust policies to enhance adaptability in the presence of adversarial observation attacks. DTS is utilized to optimally transition between robust models, mitigating the overall distributional shift in value estimation under adversarial perturbations. The theoretical framework is derived which states the optimality of DTS based switching and inducing antifragile behaviour against unseen adversarial attacks.

The proposed DTS-based antifragile RL approach is evaluated against progressively stronger adversarial attacks, including hijacking-induced spoofing, and benchmarked against conventional robust and standard RL techniques. The key findings of this study are as follows.

- **Non-stationarity of action robust policies under adversarial attacks:** Analyzing various robust models under escalating adversarial attacks reveals that a single robust model does not maintain optimal performance across different attack intensities. This underscores the necessity of dynamic policy switching to achieve optimal resilience.
- **Enhanced Robustness Against Strong PGD Adversarial Attacks:** The DTS-based antifragile RL algorithm outperforms standard and benchmark robust RL methods in countering stronger Projected Gradient Descent (PGD) attacks, particularly in terms of minimizing navigation path lengths with average reward improvement of 50% and increased average number of conflict-free trajectories by around 5% with respect to adversarial RL and 10% with respect to probabilistic robust RL.
- **Navigation Resilience to Spoofing Attacks:** The proposed antifragile RL approach demonstrates superior resilience to previously unseen spoofing attacks compared to robust and standard RL models. This highlights the core principle of antifragility, in which a system trained under weaker adversarial conditions exhibits the capacity to counter unforeseen attack scenarios effectively.

Future research will focus on extending this antifragility framework to multi-UAV navigation scenarios, further en-

hancing its applicability in complex multi-agent adversarial airspace environments.

REFERENCES

- [1] H. Huang and A. V. Savkin, "Aerial surveillance in cities: When uavs take public transportation vehicles," *IEEE Transactions on Automation Science and Engineering*, vol. 20, no. 2, pp. 1069–1080, 2022.
- [2] Y.-J. Zheng, Y.-C. Du, H.-F. Ling, W.-G. Sheng, and S.-Y. Chen, "Evolutionary collaborative human-uav search for escaped criminals," *IEEE Transactions on Evolutionary Computation*, vol. 24, no. 2, pp. 217–231, 2019.
- [3] W. Zhang, K. Song, X. Rong, and Y. Li, "Coarse-to-fine uav target tracking with deep reinforcement learning," *IEEE Transactions on Automation Science and Engineering*, vol. 16, no. 4, pp. 1522–1530, 2018.
- [4] K. Obermeyer, "Path planning for a uav performing reconnaissance of static ground targets in terrain," in *AIAA Guidance, Navigation, and Control Conference*, 2009, p. 5888.
- [5] D. Dissanayaka, T. R. Wanasinghe, O. De Silva, A. Jayasiri, and G. K. Mann, "Review of navigation methods for uav-based parcel delivery," *IEEE Transactions on Automation Science and Engineering*, vol. 21, no. 1, pp. 1068–1082, 2023.
- [6] S. Huang, R. S. H. Teo, and K. K. Tan, "Collision avoidance of multi unmanned aerial vehicles: A review," *Annual Reviews in Control*, vol. 48, pp. 147–164, 2019.
- [7] P. Kopardekar, J. Rios, T. Prevot, M. Johnson, J. Jung, and J. E. Robinson, "Unmanned aircraft system traffic management (utm) concept of operations," in *AIAA AVIATION Forum and Exposition*, 2016.
- [8] O. de l'aviation civile internationale, *Global air traffic management operational concept*. ICAO, 2005.
- [9] Y. Tang and Y. Xu, "Incorporating optimization in strategic conflict resolution for uas traffic management," *IEEE Transactions on Intelligent Transportation Systems*, 2023.
- [10] C. Huang, I. Petrunin, and A. Tsourdos, "Strategic conflict management using recurrent multi-agent reinforcement learning for urban air mobility operations considering uncertainties," *J Intell Robot Syst*, 2023.
- [11] A. Hamissi and A. Dhraief, "A survey on the unmanned aircraft system traffic management," *ACM Computing Surveys*, vol. 56, no. 3, pp. 1–37, 2023.
- [12] C. Huang, I. Petrunin, and A. Tsourdos, "Dynamic graph propagation for performance-based tactical conflict resolution in urban air mobility," in *2023 International Conference on Unmanned Aircraft Systems (ICUAS)*, 2023, pp. 152–158. DOI: [10.1109/ICUAS57906.2023.10156320](https://doi.org/10.1109/ICUAS57906.2023.10156320).
- [13] J. N. Yasin, S. A. Mohamed, M.-H. Haghbayan, J. Heikkonen, H. Tenhunen, and J. Plosila, "Unmanned aerial vehicles (uavs): Collision avoidance systems and approaches," *IEEE Access*, vol. 8, pp. 105 139–105 155, 2020.
- [14] P. Zhao and Y. Liu, "Physics informed deep reinforcement learning for aircraft conflict resolution," *IEEE Transactions on Intelligent Transportation Systems*, vol. 23, no. 7, pp. 8288–8301, 2021.
- [15] Y. Li, Y. Zhang, T. Guo, Y. Liu, Y. Lv, and W. Du, "Graph reinforcement learning for multi-aircraft conflict resolution," *IEEE Transactions on Intelligent Vehicles*, 2024.
- [16] Z. Yu, Z. Wang, J. Yu, D. Liu, H. H. Song, and Z. Li, "Cybersecurity of unmanned aerial vehicles: A survey," *IEEE Aerospace and Electronic Systems Magazine*, vol. 39, no. 9, pp. 182–215, 2023.
- [17] G. Apruzzese, M. Andreolini, M. Marchetti, A. Venturi, and M. Colajanni, "Deep reinforcement adversarial learning against botnet evasion attacks," *IEEE Transactions on Network and Service Management*, vol. 17, no. 4, pp. 1975–1987, 2020.
- [18] D. K. Panda and W. Guo, "Fragility impact of rl based advanced air mobility under gradient attacks and packet drop constraints," in *2023 IEEE 98th Vehicular Technology Conference (VTC2023-Fall)*, IEEE, 2023, pp. 1–7.
- [19] K.-F. Chu and W. Guo, "Multi-agent reinforcement learning-based passenger spoofing attack on mobility-as-a-service," *IEEE Transactions on Dependable and Secure Computing*, pp. 1–17, 2024. DOI: [10.1109/TDSC.2024.3379283](https://doi.org/10.1109/TDSC.2024.3379283).
- [20] K.-F. Chu, H. Yuan, J. Yuan, W. Guo, N. Balta-Ozkan, and S. Li, "A survey of artificial intelligence-related cybersecurity risks and countermeasures in mobility-as-a-service," *IEEE Intelligent Transportation Systems Magazine*, pp. 2–20, 2024. DOI: [10.1109/MITS.2024.3427655](https://doi.org/10.1109/MITS.2024.3427655).
- [21] X. Wei, J. Ma, and C. Sun, "A survey on security of unmanned aerial vehicle systems: Attacks and countermeasures," *IEEE Internet of Things Journal*, 2024.
- [22] W. Guan and K. Wang, "Autonomous collision avoidance of unmanned surface vehicles based on improved a-star and dynamic window approach algorithms," *IEEE Intelligent Transportation Systems Magazine*, vol. 15, no. 3, pp. 36–50, 2023.
- [23] T. Zhang, M. Fu, W. Song, Y. Yang, and M. Wang, "Trajectory planning based on spatio-temporal map with collision avoidance guaranteed by safety strip," *IEEE Transactions on Intelligent Transportation Systems*, vol. 23, no. 2, pp. 1030–1043, 2020.
- [24] J. Sun, J. Tang, and S. Lao, "Collision avoidance for cooperative uavs with optimized artificial potential field algorithm," *IEEE Access*, vol. 5, pp. 18 382–18 390, 2017.
- [25] J. Ji, A. Khajepour, W. W. Melek, and Y. Huang, "Path planning and tracking for vehicle collision avoidance based on model predictive control with multiconstraints," *IEEE Transactions on Vehicular Technology*, vol. 66, no. 2, pp. 952–964, 2016.
- [26] A. Alonso-Ayuso, L. F. Escudero, and F. J. Martín-Campo, "Collision avoidance in air traffic management: A mixed-integer linear optimization approach," *IEEE Transactions on Intelligent Transportation Systems*, vol. 12, no. 1, pp. 47–57, 2010.
- [27] P. Yao, H. Wang, and Z. Su, "Uav feasible path planning based on disturbed fluid and trajectory propagation," *Chinese Journal of Aeronautics*, vol. 28, no. 4, pp. 1163–1177, 2015.
- [28] P. Yao, H. Wang, and Z. Su, "Real-time path planning of unmanned aerial vehicle for target tracking and obstacle avoidance in complex dynamic environment," *Aerospace Science and Technology*, vol. 47, pp. 269–279, 2015.
- [29] D. Celestini, S. Primatesta, and E. Capello, "Trajectory planning for uavs based on interfered fluid dynamical system and bézier curves," *IEEE Robotics and Automation Letters*, vol. 7, no. 4, pp. 9620–9626, 2022.
- [30] Y. Zhang and H. Wang, "Adaptive interfered fluid dynamic system algorithm based on deep reinforcement learning framework," in *International Conference on Autonomous Unmanned Systems*, Springer, 2021, pp. 1388–1397.
- [31] I. Iahi *et al.*, "Challenges and countermeasures for adversarial attacks on deep reinforcement learning," *IEEE Transactions on Artificial Intelligence*, vol. 3, no. 2, pp. 90–109, 2021.
- [32] K.-F. Chu, H. Yuan, J. Yuan, W. Guo, N. Balta-Ozkan, and S. Li, "A survey of artificial intelligence-related cybersecurity risks and countermeasures in mobility-as-a-service," *IEEE Intelligent Transportation Systems Magazine*, 2024.
- [33] A. Pattanaik, Z. Tang, S. Liu, G. Bommannan, and G. Chowdhary, "Robust deep reinforcement learning with adversarial attacks," in *17th International Conference on Autonomous Agents and Multiagent Systems, AAMAS 2018*, International Foundation for Autonomous Agents and Multiagent Systems (IFAAMAS), 2018, pp. 2040–2042.
- [34] N. Papernot, P. McDaniel, S. Jha, M. Fredrikson, Z. B. Celik, and A. Swami, "The limitations of deep learning in adversarial

- settings,” in *2016 IEEE European symposium on security and privacy (EuroS&P)*, IEEE, 2016, pp. 372–387.
- [35] X. Y. Lee, S. Ghadai, K. L. Tan, C. Hegde, and S. Sarkar, “Spatiotemporally constrained action space attacks on deep reinforcement learning agents,” in *Proceedings of the AAAI conference on artificial intelligence*, vol. 34, 2020, pp. 4577–4584.
- [36] M. Huai, J. Sun, R. Cai, L. Yao, and A. Zhang, “Malicious attacks against deep reinforcement learning interpretations,” in *Proceedings of the 26th ACM SIGKDD International Conference on Knowledge Discovery & Data Mining*, 2020, pp. 472–482.
- [37] Y. Han *et al.*, “Reinforcement learning for autonomous defence in software-defined networking,” in *Decision and Game Theory for Security: 9th International Conference, GameSec 2018, Seattle, WA, USA, October 29–31, 2018, Proceedings 9*, Springer, 2018, pp. 145–165.
- [38] V. Behzadan and A. Munir, “Whatever does not kill deep reinforcement learning, makes it stronger,” *arXiv e-prints*, arXiv-1712, 2017.
- [39] N. Papernot, P. McDaniel, X. Wu, S. Jha, and A. Swami, “Distillation as a defense to adversarial perturbations against deep neural networks,” in *2016 IEEE symposium on security and privacy (SP)*, IEEE, 2016, pp. 582–597.
- [40] F. Delgrange, A. Nowé, and G. A. Pérez, “Distillation of rl policies with formal guarantees via variational abstraction of markov decision processes,” in *Proceedings of the AAAI Conference on Artificial Intelligence*, vol. 36, 2022, pp. 6497–6505.
- [41] X. Pan, D. Seita, Y. Gao, and J. Canny, “Risk averse robust adversarial reinforcement learning,” in *2019 International Conference on Robotics and Automation (ICRA)*, IEEE, 2019, pp. 8522–8528.
- [42] C. Tessler, Y. Efroni, and S. Mannor, “Action robust reinforcement learning and applications in continuous control,” in *International Conference on Machine Learning*, PMLR, 2019, pp. 6215–6224.
- [43] J. Wang, Y. Liu, and B. Li, “Reinforcement learning with perturbed rewards,” in *Proceedings of the AAAI conference on artificial intelligence*, vol. 34, 2020, pp. 6202–6209.
- [44] L. Pinto, J. Davidson, R. Sukthankar, and A. Gupta, “Robust adversarial reinforcement learning,” in *International conference on machine learning*, PMLR, 2017, pp. 2817–2826.
- [45] H. Zhang, H. Chen, D. Boning, and C. J. Hsieh, “Robust reinforcement learning on state observations with learned optimal adversary,” in *9th International Conference on Learning Representations, ICLR 2021*, 2021.
- [46] N. N. Taleb and R. Douady, “Mathematical definition, mapping, and detection of (anti) fragility,” *Quantitative Finance*, vol. 13, no. 11, pp. 1677–1689, 2013.
- [47] L. Sun, M. Makridis, A. Genser, C. Axenie, M. Grossi, and A. Kouvelas, “Exploring antifragility in traffic networks: Anticipating and gaining from disruptions with reinforcement learning,” in *103rd Annual Meeting of the Transportation Research Board (TRB 2024)*, 2024.
- [48] C. Axenie and M. Saveriano, “Antifragile control systems: The case of mobile robot trajectory tracking under uncertainty and volatility,” *IEEE Access*, 2023.
- [49] C. Pravin, I. Martino, G. Nicosia, and V. Ojha, “Fragility, robustness and antifragility in deep learning,” *Artificial Intelligence*, vol. 327, p. 104060, 2024.
- [50] A. T. Altun, Y. Xu, G. Inalhan, and M. W. Hardt, “Analyzing fragility of the advanced air mobility system and exploring antifragile networks,” in *2023 IEEE/AIAA 42nd Digital Avionics Systems Conference (DASC)*, IEEE, 2023, pp. 1–8.
- [51] H. de Bruijn, A. Groessler, and N. Videira, “Antifragility as a design criterion for modelling dynamic systems,” *Systems Research and Behavioral Science*, vol. 37, no. 1, pp. 23–37, 2020.
- [52] S. Han and Y. Sung, “A max-min entropy framework for reinforcement learning,” *Advances in Neural Information Processing Systems*, vol. 34, pp. 25 732–25 745, 2021.
- [53] B. Eysenbach and S. Levine, “Maximum entropy rl (provably) solves some robust rl problems,” in *10th International Conference on Learning Representations, ICLR 2022*, 2022.
- [54] J. Chen, D. Zhou, J. Yi, and Q. Gu, “A frank-wolfe framework for efficient and effective adversarial attacks,” in *Proceedings of the AAAI conference on artificial intelligence*, vol. 34, 2020, pp. 3486–3494.
- [55] H. Gupta, K. H. Jin, H. Q. Nguyen, M. T. McCann, and M. Unser, “Cnn-based projected gradient descent for consistent ct image reconstruction,” *IEEE Transactions on Medical Imaging*, vol. 37, no. 6, pp. 1440–1453, 2018.
- [56] S. Agrawal and N. Goyal, “Analysis of thompson sampling for the multi-armed bandit problem,” in *Conference on learning theory, JMLR Workshop and Conference Proceedings*, 2012, pp. 39–1.
- [57] Q. Wu, N. Iyer, and H. Wang, “Learning contextual bandits in a non-stationary environment,” in *The 41st International ACM SIGIR Conference on Research & Development in Information Retrieval*, 2018, pp. 495–504.
- [58] S. Agrawal and N. Goyal, “Near-optimal regret bounds for thompson sampling,” *Journal of the ACM (JACM)*, vol. 64, no. 5, pp. 1–24, 2017.
- [59] *Uav obstacle avoiding drl*, https://github.com/ZYunfeii/UAV_Obstacle_Avoiding_DRL/tree/master, [Accessed 25-08-2024], 2023.
- [60] C. Dann, Y. Mansour, M. Mohri, A. Sekhari, and K. Sridharan, “Guarantees for epsilon-greedy reinforcement learning with function approximation,” in *International conference on machine learning*, PMLR, 2022, pp. 4666–4689.
- [61] A. Garivier and E. Moulines, “On upper-confidence bound policies for switching bandit problems,” in *International conference on algorithmic learning theory*, Springer, 2011, pp. 174–188.
- [62] J. Ho and S. Ermon, “Generative adversarial imitation learning,” *Advances in neural information processing systems*, vol. 29, 2016.
- [63] S. M. Giray, “Anatomy of unmanned aerial vehicle hijacking with signal spoofing,” in *2013 6th International Conference on Recent Advances in Space Technologies (RAST)*, IEEE, 2013, pp. 795–800.
- [64] Y.-P. Hsieh, C. Liu, and V. Cevher, “Finding mixed nash equilibria of generative adversarial networks,” in *International Conference on Machine Learning*, PMLR, 2019, pp. 2810–2819.
- [65] P. Kamalaruban, Y.-T. Huang, Y.-P. Hsieh, P. Rolland, C. Shi, and V. Cevher, “Robust reinforcement learning via adversarial training with langevin dynamics,” *Advances in Neural Information Processing Systems*, vol. 33, pp. 8127–8138, 2020.
- [66] C. A. Bhardwaj, “Adaptively preconditioned stochastic gradient langevin dynamics,” *arXiv preprint arXiv:1906.04324*, 2019.
- [67] L. Luo, Y. Xiong, Y. Liu, and X. Sun, “Adaptive gradient methods with dynamic bound of learning rate,” in *International Conference on Learning Representations*, 2019.
- [68] F. Zou, L. Shen, Z. Jie, W. Zhang, and W. Liu, “A sufficient condition for convergences of adam and rmsprop,” in *Proceedings of the IEEE/CVF Conference on computer vision and pattern recognition*, 2019, pp. 11 127–11 135.
- [69] Y. Duan, X. Chen, R. Houthoofd, J. Schulman, and P. Abbeel, “Benchmarking deep reinforcement learning for continuous control,” in *International conference on machine learning*, PMLR, 2016, pp. 1329–1338.

APPENDIX A
INTERFERED FLOW FIELD

The interfered flow field is the modification of the flow field that affects the initial flow field due to the presence of obstacles. The 3D obstacle is designed as a standard convex polyhedron, as:

$$\Gamma(\mathbf{P}) = \left(\frac{x-x_0}{\check{a}}\right)^{2\check{p}} + \left(\frac{y-y_0}{\check{b}}\right)^{2\check{q}} + \left(\frac{z-z_0}{\check{c}}\right)^{2\check{r}}. \quad (\text{A.1})$$

In this case, $\check{p}, \check{q}, \check{r}, \check{a}, \check{b}, \check{c}$ determine the shape of the convex polyhedron of the obstacle, and (x_0, y_0, z_0) determine centre of the convex polyhedron. If we consider N obstacles in the space, the interfered flow field is represented by a disturbance matrix as:

$$\bar{\mathbf{M}}(\mathbf{P}) = \sum_{n=1}^N \mathfrak{w}_n(\mathbf{P}) M_n(\mathbf{P}), \quad (\text{A.2})$$

where \mathfrak{w} is the disturbance weighting factor for the N obstacles defined as:

$$\mathfrak{w}_n(\mathbf{P}) = \begin{cases} 1 & N=1, \\ \prod_{i=1, i \neq n}^N \frac{\Gamma_i(\mathbf{P})-1}{\Gamma_i(\mathbf{P})-1+\Gamma_n(\mathbf{P})-1}. \end{cases} \quad (\text{A.3})$$

Here we define the radial normal vector along the 3D obstacle \mathbf{t}_n as:

$$\mathbf{t}_n(\mathbf{P}) = \begin{bmatrix} \frac{\partial \Gamma_n(\mathbf{P})}{\partial x} & \frac{\partial \Gamma_n(\mathbf{P})}{\partial y} & \frac{\partial \Gamma_n(\mathbf{P})}{\partial z} \end{bmatrix}. \quad (\text{A.4})$$

We consider two vectors $h_{n,1}(\mathbf{P}), h_{n,2}(\mathbf{P})$ which are orthogonal to the radial vector \mathbf{t}_n and also mutually orthogonal to each other, given as:

$$h_{n,1}(\mathbf{P}) = \begin{bmatrix} \frac{\partial \Gamma_n(\mathbf{P})}{\partial y} \\ -\frac{\partial \Gamma_n(\mathbf{P})}{\partial x} \\ 0 \end{bmatrix}^T, \quad (\text{A.5})$$

$$h_{n,2}(\mathbf{P}) = \begin{bmatrix} \frac{\partial \Gamma_n(\mathbf{P})}{\partial x} \cdot \frac{\partial \Gamma_n(\mathbf{P})}{\partial z} \\ \frac{\partial \Gamma_n(\mathbf{P})}{\partial x} \cdot \frac{\partial \Gamma_n(\mathbf{P})}{\partial z} \\ -\left(\frac{\partial \Gamma_n(\mathbf{P})}{\partial x}\right)^2 - \left(\frac{\partial \Gamma_n(\mathbf{P})}{\partial y}\right)^2 \end{bmatrix}^T.$$

The plane S formed by $h_{n,1}(\mathbf{P}), h_{n,2}(\mathbf{P})$ is perpendicular to \mathbf{t}_n . Hence, we can write any unit vector on the plane S as,

$$[\cos \vartheta_n \quad \sin \vartheta_n \quad 0], \quad (\text{A.6})$$

where ϑ_n is the direction coefficient affecting the tangential disturbance. The disturbance matrix while considering a single obstacle is given as:

$$\mathbf{M}_n(\mathbf{P}) = \mathbf{M}_{n1}(\mathbf{P}) + \mathbf{M}_{n2}(\mathbf{P}),$$

$$\mathbf{M}_n = \mathbf{I} - \frac{\mathbf{t}_n(\mathbf{P}) \mathbf{t}_n(\mathbf{P})^T}{|\Gamma_n(\mathbf{P})|^{\frac{1}{\rho_n}} \mathbf{t}_n(\mathbf{P})^T \mathbf{t}_n(\mathbf{P})} + \frac{h_n(\mathbf{P}) \mathbf{t}_n(\mathbf{P})^T}{|\Gamma_n(\mathbf{P})|^{\frac{1}{\zeta_n}} h_n(\mathbf{P})^T \mathbf{t}_n(\mathbf{P})}. \quad (\text{A.7})$$

Here we can define ρ_n and ζ_n using the given formulas,

$$\begin{cases} \rho_n = \rho_0 \cdot \exp\left(1 - \frac{1}{d(P,P_d)d(P,O_n)}\right), \\ \zeta_n = \zeta_0 \cdot \exp\left(1 - \frac{1}{d(P,P_d)d(P,O_n)}\right). \end{cases} \quad (\text{A.8})$$

Here, $d(\mathbf{P}, O_n)$ represents the distance between the end of the path and the surface of the N -th obstacle, ρ_0, ζ_0 represents

the response coefficient of the obstacle. The dynamic obstacle speed threat is represented as

$$v_{\text{obs}}(\mathbf{P}) = \sum_{n=1}^N \mathfrak{w}_n(\mathbf{P}) \exp\left[\frac{-\Gamma_n(\mathbf{P})}{\Upsilon}\right] V_{\text{obs}}^n(\mathbf{P}). \quad (\text{A.9})$$

where V_n^{obs} is considered as the moving speed of the N th obstacle, Υ is a constant greater than zero.

APPENDIX B
SAMPLING BASED SOLUTION FOR ROBUST RL

Sampling-based methods are employed to derive the mixed Nash equilibrium from the objective function in (10), as outlined in [64]. This equilibrium is then utilized to address RL challenges [65]. In order to avoid the saddle points, isotropic gradient noise is introduced into the stochastic gradient descent (SGD) process used to minimize the loss functions during the training of agent and adversarial policy networks. By adaptively scaling this noise as per higher-order curvature measures, such as Fisher scoring, the noise can be pre-conditioned to achieve improved convergence properties [66]. When optimizing the loss function using SGD concerning the parameter Θ , the update equation at each step is given by:

$$\hat{\mathbf{g}}_s(\Theta_t) \leftarrow \nabla_{\Theta} \hat{\mathcal{L}}_s(\Theta_t). \quad (\text{B.1})$$

Here, $\hat{\mathcal{L}}_s(\Theta_t)$ represents the stochastic estimate of the loss function. Hence, the update equation can be represented as:

$$\Theta_{t+1} \leftarrow \Theta_t - \eta (\hat{\mathbf{g}}_s(\Theta_t)). \quad (\text{B.2})$$

Incorporating Gaussian noise in the parametric update $\mathcal{N}(0, \epsilon)$:

$$\begin{aligned} \zeta_t &\sim \mathcal{N}(0, \epsilon), \\ \Theta_{t+1} &\leftarrow \Theta_t - \eta (\hat{\mathbf{g}}_s(\Theta_t) + \zeta_t). \end{aligned} \quad (\text{B.3})$$

The uniform scaling of noise can lead to improper parameter update scaling, potentially slowing the algorithm's training speed and resulting in convergence to suboptimal minima [67]. In order to issue this, adaptive preconditioners are employed, such as RMSProp [68], which approximates the inverse of the second-order moments of the gradient update using a diagonal matrix. Bhardwaj et al. [66] propose an adaptive preconditioned noise that takes advantage of a diagonal approximation of the second-order gradient updates' moments to enhance the training efficiency of first-order methods. Consequently, noise scaling is adjusted proportionally to accelerate training as follows:

$$\begin{aligned} \mathbf{C}_t &\leftarrow \rho \mathbf{C}_{t-1} + (1-\rho) (\hat{\mathbf{g}}_s(\Theta_t) - \boldsymbol{\mu}_t) (\hat{\mathbf{g}}_s(\Theta_t) - \boldsymbol{\mu}_{t-1}), \\ \zeta_t &\sim \mathcal{N}(\boldsymbol{\mu}_t, \mathbf{C}_t), \\ \Theta_{t+1} &\leftarrow \Theta_t - \eta (\hat{\mathbf{g}}_s(\Theta_t) + \psi \zeta_t). \end{aligned} \quad (\text{B.4})$$

In equation (B.4), we observe that the noise covariance preconditioner, scales the noise proportionally along the dimensions with larger gradients. This approach helps to escape saddle points and navigate the policy space more effectively while dealing with broader loss minima, ultimately leading to faster convergence and improved solutions. Therefore, incorporating adaptive noise into the loss function allows optimization of both the critic loss and the agent and adversarial policy loss

functions. If α_i as the adversarial contribution, then the general action a_t is expressed as follows:

$$a_t = \alpha_i v_\omega(\Phi_t) + (1 - \alpha_i) \pi_\theta(\Phi_t). \quad (\text{B.5})$$

If we consider a batch of samples $B = \{(\Phi_t, a_t, r_t, \Phi', \mathfrak{d})\}$ from the replay buffer \mathcal{D} , then we compute the critic target y_{targ} as follows:

$$y_{\text{targ}} = r_t + \gamma(1 - \mathfrak{d}) Q_{\phi_{\text{targ}}}(\Phi', (1 - \alpha_i) \mu_\theta + \alpha_i v_\omega). \quad (\text{B.6})$$

Thus target y_{targ} can be utilized to formulate the critic loss function as,

$$L(\phi) = \frac{1}{N} \sum_{B=\{(\Phi_t, a_t, r_t, \Phi', \mathfrak{d})\}} (y(r, \Phi', d) - Q_\phi(\phi, a))^2. \quad (\text{B.7})$$

We can also compute the agent and adversary policy updates as:

$$\begin{aligned} \nabla_\theta J(\widehat{\theta}, \widehat{\omega}_t) &= \frac{1 - \alpha_i}{N} \sum_{\Phi \in \mathcal{D}} \nabla_\theta \mu_\theta(\Phi) \nabla_a Q_\phi(\Phi, a), \\ \nabla_\omega J(\widehat{\theta}_t, \widehat{\omega}) &= \frac{\alpha_i}{N} \sum_{\Phi \in \mathcal{D}} \nabla_\omega v_\omega(\Phi) \nabla_a Q_\phi(\Phi, a). \end{aligned} \quad (\text{B.8})$$

To minimize the loss functions of critics and policy given by equations (B.6) and (B.7) respectively, we incorporate SGLD noise into the update equations as specified in (B.4). This approach is taken to update the joint critic parameters ϕ and the agent and adversary policy parameters $\{\theta, \omega\}$. If we consider $\mathbf{g} = \{\nabla_\theta J, \nabla_\omega J\}$, $\boldsymbol{\mu}_t = \{\mu_\theta, \mu_\omega\}$, $\mathbf{C}_t = \{C_\theta, C_\omega\}$ according to the dynamics of SGLD given in (B.4), the update equation for the agent and the adversary parameter to obtain the mixed Nash equilibrium for the max-min objective in (10) for the k^{th} sample from the buffer at time t , is given as:

$$\theta_t^{k+1} \leftarrow \theta_t^k + \eta \left(\nabla_\theta J(\widehat{\theta}, \widehat{\omega}_t) + \boldsymbol{\psi} \xi_t \right), \quad (\text{B.9})$$

$$\omega_t^{k+1} \leftarrow \omega_t^k - \eta \left(\nabla_\omega J(\widehat{\theta}, \widehat{\omega}_t) + \boldsymbol{\psi} \xi_t \right). \quad (\text{B.10})$$

Here $\boldsymbol{\psi}$ represents the noise parameter. The parameters updated with the time t is given by

$$\bar{\omega}_t = (1 - \beta) \bar{\omega}_t + \beta \omega_t^{(k+1)}; \quad \bar{\theta}_t = (1 - \beta) \bar{\theta}_t + \beta \theta_t^{(k+1)}. \quad (\text{B.11})$$

Obtain the parameters for the next time duration as,

$$\omega_{t+1} = (1 - \beta) \omega_t + \beta \bar{\omega}_t; \quad \theta_{t+1} = (1 - \beta) \theta_t + \beta \bar{\theta}_t. \quad (\text{B.12})$$

The overall training algorithm to obtain an ensemble set of agent and adversarial policy networks is explained in Algorithm 1.

Algorithm 1 Ensemble Adversarial Action Robust RL

Initialize: Policy parameters ω, θ and Q function parameter ϕ .

Initialize: The target network parameters $\omega_{\text{targ}} \leftarrow \omega_1, \theta_{\text{targ}} \leftarrow \theta_1$, and $\chi_{\text{targ}} \leftarrow \chi$.

Initialize: Replay buffer

Initialize: Ensemble Policy Set $\mathcal{P} \leftarrow \emptyset$ and Ensemble Critic Set $\mathcal{Q} \leftarrow \emptyset$

Initialize: $\alpha_i \leftarrow 0.1$

Initialize: $t \leftarrow 1$.

repeat

- 1: Observe state Φ , select the actions according to $\rho_{\text{agent}} = \mu_\theta + \zeta$, $\rho_{\text{adv}} = v_\omega + \zeta'$ where $\zeta, \zeta' \sim \mathcal{N}(0, \sigma I)$.
- 2: Execute the action $\rho_t = \alpha_i \cdot \rho_{\text{adv}} + (1 - \alpha_i) \cdot \rho_{\text{agent}}$ in the environment.
- 3: Observe the reward r in (8), obtain the next state Φ' according to (3) and check whether the UAV has reached its destination using the signal done d .
- 4: Store $(\Phi, \rho, r, \Phi', d)$ in the replay buffer \mathcal{D} .
- 5: Reset the environment if the state Φ' is terminal.
- 6: **if** its time to update agent and adversary model **then**
- 7: $\omega_t, \omega_t^{(1)} \leftarrow \omega_t, \theta_t^{(1)} \leftarrow \theta_t$
- 8: **for** $k = 1, 2, \dots, K_t$ **do**
- 9: Sample a random minibatch of N transitions $B = \{(\Phi, \bar{\rho}, r, \Phi', d)\}$ from \mathcal{D} .
- 10: Compute the targets as per (B.6).
- 11: Compute the loss function to update the joint critic $\nabla_\phi L(\phi)$ as per (B.7).
- 12: Compute the agent and adversary policy gradient according to (B.8).
- 13: Compute the agent and adversary parameters as per (B.8).
- 14: Update the parameters of the agent and adversary network $\{\theta, \omega\}$ according to (B.9) and (B.10).
- 15: Obtain the value of $\{\bar{\theta}, \bar{\omega}\}$ according to (B.11).
- 16: Update the parameters of the target network used to compute the target according to (B.9).

$$\begin{aligned} \phi_{\text{targ}} &\leftarrow \tau \phi_{\text{targ}} + (1 - \tau) \phi \\ \theta_{\text{targ}} &\leftarrow \tau \theta_{\text{targ}} + (1 - \tau) \theta_t^{k+1} \\ \omega_{\text{targ}} &\leftarrow \tau \omega_{\text{targ}} + (1 - \tau) \omega_t^{k+1} \end{aligned} \quad (\text{B.13})$$

17: **end for**

18: Update $\{\omega_{t+1}, \theta_{t+1}\}$ as per (B.12).

19: $t \leftarrow t + 1$

20: **end if**

21: **until** Max Episodes Reached.

22: Obtain $\Delta \mathbf{H} = \mathbb{E} \left[\Delta \mathbf{H}_{\alpha_i}^{\text{rand}} - \max \left[\mathbf{H}_{\alpha_i}^{\text{opt}} \right] \right]$.

23: **if** $\Delta \mathbf{H} > \mathbf{H}^{\text{th}}$ **then**

$$\begin{aligned} \alpha_i &\leftarrow \alpha_i + 0.1, \\ \mathcal{P}' &\leftarrow \mathcal{P} \cup \{\theta, \omega\}_{\alpha_i}, \\ \mathcal{Q}' &\leftarrow \mathcal{Q} \cup \{\phi\}_{\alpha_i}, \\ \mathcal{P} &\leftarrow \mathcal{P}', \\ \mathcal{Q} &\leftarrow \mathcal{Q}'. \end{aligned} \quad (\text{B.14})$$

24: **else End**

25: **end if**

Output: Ensemble Policy set \mathcal{P} and critic set \mathcal{Q} .

APPENDIX C

ALGORITHM FOR GENERATING ADVERSARIAL STATES

Algorithm 2 Generate adversarial state Φ^{adv} for obtaining the distributional shift from vanilla and robust policies

Input Current State Φ , Step size α , maximum perturbation ε , mean observation $\check{\mu}_\Phi$, standard deviation of observation $\check{\sigma}_\Phi$.

Output Adversarial State Φ^{adv}

- 1: Calculate normalized state $\Phi_{\text{norm}} = (\Phi - \check{\mu}_\Phi) / \check{\sigma}_\Phi$.
- 2: Compute the perturbed input $\delta_0 = 2\varepsilon \cdot \mathcal{U}(-0.5, 0.5)$.
- 3: **for** $k = 0, \dots, N-1$ **do**
- 4: Compute the step size $F = c/k + c$.
- 5: Obtained the perturbed state $\Phi_k = \Phi_{\text{norm}} + \delta_0$.
- 6: Obtain the gradient of the actor loss on perturbed state $g_k = \nabla_{\Phi_k} \mathcal{L}_\pi(\Phi_k)$.
- 7: Compute the perturbation step $s_k = \varepsilon \cdot \text{sign}(g_k)$.
- 8: Update the perturbation $\delta_{k+1} = F_k s_k + (1 - F_k) \delta_k$.
- 9: **end for**
- 10: Compute the final adversarial example in normalized form $\Phi_{\text{adv}}^{\text{norm}} = \Phi_{\text{norm}} + \delta_N$.
- 11: Renormalize to obtain the final adversarial state $\Phi^{\text{adv}} = \check{\sigma}_\Phi \cdot \Phi_{\text{adv}}^{\text{norm}} + \check{\mu}_\Phi$.

APPENDIX D

ALGORITHM FOR DISCOUNTED THOMPSON SAMPLING

The algorithm for DTS is provided as follows:

Algorithm 3 Discounted Thompson Sampling for Switching Robust Policies against Adversarial Attacks

Parameters $\eta \in (0, 1]$, $\alpha_0, \mathbf{b}_0 \in \mathbb{R}_{\geq 0}$, $K = |\mathcal{A}| \geq 2$

- 1: Initialize $\mathfrak{S}_k, \mathfrak{F}_k = 0 \forall k \in \{1, \dots, K\}$.
- 2: **for** $t = 1, \dots, T$ **do**
- 3: **for** $k = 1, \dots, K$ **do** $\Lambda_k(t) \sim \mathfrak{B}(\mathfrak{S}_k + \alpha_0, \mathfrak{F}_k + \mathbf{b}_0)$.
- 4: **end for**
- 5: Play arm $I_t^\mathcal{A} := \arg \max_k \Lambda_k(t)$ and observe the Bernoulli reward \tilde{r}_t from the true probabilities p_{true} .
- 6: Perform a Bernoulli trial with success probability \tilde{r}_t and observe output \tilde{r}_t .
- 7: Update $\mathfrak{S}_{I_t^\mathcal{A}} \leftarrow \eta \mathfrak{S}_{I_t^\mathcal{A}} + \tilde{r}_t$ and $\mathfrak{F}_{I_t^\mathcal{A}} \leftarrow \eta \mathfrak{F}_{I_t^\mathcal{A}} + (1 - \tilde{r}_t)$.
- 8: Update $\mathfrak{S}_k \leftarrow \eta \mathfrak{S}_k$ and $\mathfrak{F}_k \leftarrow \eta \mathfrak{F}_k; \forall k \neq I_t^\mathcal{A}$.
- 9: **end for**

APPENDIX E

BENCHMARKING ALGORITHMS

Benchmarking is performed by evaluating the standard policy gradient algorithm, such as the DDPG, along with its robust variants. An approach involves an agent who intends to execute an action \mathbf{a} , but an alternative adversarial action $\bar{\mathbf{a}}$ is implemented with probability α . Another variant, conceptually similar to the approach described in Section E.II, employs soft probabilistic robust policy iteration (PR-PI) as proposed in [42], rather than solving the mixed Nash equilibrium objective in (10). The final benchmarking strategy involves training the agent to optimize the rewards without directly modifying the policy during training. Instead, an adversarial buffer is utilized, allowing the agent to learn the optimal value function in the

presence of adversarial states. A brief explanation of these algorithms is provided in the subsequent subsections.

A. Deep Deterministic Policy Gradient (DDPG)

The schematic shown in Figure 3, the action robust RL is replaced by DDPG considering $\alpha = 0$. Hence, the critic target y_{targ} in (B.6) is modified as follows,

$$y_{\text{targ}} = r_t + \gamma(1-d)Q_{\phi_{\text{targ}}}(\Phi', \mu_\theta). \quad (\text{E.1})$$

Similarly the policy loss with $\alpha = 0$ shown in (B.8) to compute the policy parameter θ , will be as,

$$\nabla_{\theta} \widehat{J}(\theta) = \frac{1}{N} \sum_{\Phi \in \mathcal{D}} \nabla_{\theta} \mu_{\theta}(\Phi) \nabla_a Q_{\phi}(\Phi, a). \quad (\text{E.2})$$

Hence, the min-max objective in (10) is replaced with a pure max objective which can be solved using policy gradient methods as outlined in [69].

B. Probabilistic Robust Markov Decision Process

According to [42], PR-MDP is framed as a zero-sum game between an agent and an adversary. In this framework, an optimal probabilistic robust policy is defined with a probability α , where the adversary assumes control and executes the most detrimental actions to account for potential system control limitations and undesirable outcomes. PR-MDP addresses stochastic perturbations within the policy space. When we consider $\alpha \in [0, 1]$ and the 5-tuple MDP outlined in Section , the probabilistic joint policy $\pi_{P,\alpha}^{\text{mix}}$ is considered as

$$\pi_{P,\alpha}^{\text{mix}}(\mathbf{a}|\Phi) \equiv (1-\alpha)\pi(\mathbf{a}|\Phi) + \alpha\bar{\pi}(\mathbf{a}|\Phi). \quad (\text{E.3})$$

The $\pi_{P,\alpha}^{\text{mix}}$ to learn the optimal value function for PR-MDP is obtained using PR-PI as shown in algorithm 1 in [42].

C. Noisy Robust Markov Decision Process

According to [42], NR-MDP also models a zero-sum game between an agent and an adversary, but incorporates perturbations in the action space rather than in the policy space as in PR-MDP. Given π and $\bar{\pi}$ as the policies of the agent and the adversary, respectively, their joint policy $\pi_{P,\alpha}^{\text{mix}}$ as,

$$\pi_{N,\alpha}^{\text{mix}}(\mathbf{a}|\Phi) = \mathbb{E}_{\mathbf{b} \sim \pi(\cdot|\Phi), \bar{\mathbf{b}} \sim \bar{\pi}(\cdot|\Phi)} \left[\bar{\mathbf{I}}_{\mathbf{a}=(1-\alpha)\mathbf{b}+\alpha\bar{\mathbf{b}}} \right]. \quad (\text{E.4})$$

The NR-MDP is analogous to the Markov decision process (MDP) used to develop the ensembles, except for the addition of SGLD noise to the loss function, as described in equation (B.4) to obtain the mixed Nash equilibrium solution for the objective shown in (10). The solution to the min-max objective considered here is according to the soft PR-PI method as described in Algorithm 2 in [42].

D. Learning with Adversarial Attacks

Adversarial attacks, as proposed in [33], have been used to train DRL algorithms to address environmental uncertainties. These attacks employ the fast gradient sign method (FGSM) to introduce perturbations in the observation space. In the case of DDPG, attacks are applied considering the gradient of the policy loss function. Adversarial training is conducted within a robust control framework, where the agent is trained to handle state-space perturbations that could potentially cause the greatest impact on the reward space. The primary distinction between vanilla DDPG and adversarial DDPG lies

in the use of adversarial states by the latter in the training buffer, represented as $\mathcal{D}^{\text{adv}} = \{\Phi^{\text{adv}}, a^{\text{adv}}, \Phi', r^{\text{adv}}\}$, where the adversarial state is given by $\Phi^{\text{adv}} = \Phi + \varepsilon \cdot \text{sign}[\nabla_{\Phi} J(\theta)]$. Here, J denotes the loss of policy obtained from DDPG. In the simulation, the adversarial DDPG model was trained with $\varepsilon = 1.0$.